Two-loop QCD amplitudes for $t\bar{t}H$ production from boosted limit

Guoxing Wang ⓘ,[a,b] **Tianya Xia,**[a] **Li Lin Yang**[a] **and Xiaoping Ye**[c]

[a]*Zhejiang Institute of Modern Physics, School of Physics, Zhejiang University,*
Hangzhou 310027, China

[b]*Laboratoire de Physique Théorique et Hautes Energies (LPTHE), UMR 7589,*
Sorbonne Université et CNRS,
4 place Jussieu, 75252 Paris Cedex 05, France

[c]*School of Physics, Peking University,*
Beijing 100871, China

E-mail: wangguoxing2015@pku.edu.cn, xiatianya@zju.edu.cn,
yanglilin@zju.edu.cn, yexiaoping@pku.edu.cn

ABSTRACT: The production of a Higgs boson in association with a top-antitop quark pair ($t\bar{t}H$) holds significant importance in directly probing the top-quark Yukawa coupling, which is related to various fundamental questions in high energy physics. This paper focuses on the calculation of two-loop amplitudes for $t\bar{t}H$ production at hadron colliders in the high-energy boosted limit. The calculation employs our recently developed mass-factorization formula. To validate the accuracy of our approximate methods, we compare our results for the one-loop amplitudes and the two-loop infrared poles with the exact calculations. We then provide predictions for the finite parts of the two-loop amplitudes. By combining the contributions from real emissions, our results can be utilized to compute the next-to-next-to-leading order differential cross sections for $t\bar{t}H$ production in the high-energy boosted limit.

Contents

1 Introduction

Since the discovery of the Higgs boson by the ATLAS and CMS collaborations in 2012 [1, 2], the precision test of the properties of the Higgs boson has become one of the most important topics in high-energy physics. In particular, the Yukawa coupling between the top quark and the Higgs boson plays an important role in pursuing the answers to many deep questions, such as the origin of the masses of fundamental fermions, the stability of the electroweak vacuum, and the matter-anti-matter asymmetry in our observable universe. The ATLAS and CMS collaborations at the Large Hadron Collider (LHC) have observed the Higgs production associated with a top-antitop quark pair ($t\bar{t}H$ production) in 2018 [3, 4]. This allows us to directly probe the top-quark Yukawa coupling. The possible violation of the Charge-Parity (CP) symmetry in the coupling has also been investigated experimentally [5, 6]. With the accumulation of data in the near future, the experimental accuracy for the cross section of this process can reach 2% at the High-Luminosity LHC (HL-LHC) [7]. To match the expected precision of the HL-LHC, it is highly desirable to have equally accurate theoretical predictions.

The leading-order (LO) cross sections for $t\bar{t}H$ production were present in [8, 9]. The next-to-leading order (NLO) QCD corrections have been calculated 20 years ago [10–15] and interfaced with parton showers in [16–18]. The NLO eletroweak (EW) corrections were

reported in [19–21]. The off-shell effects of the top quark and/or the Higgs boson were considered in [22–25]. The resummation of soft-gluon contributions close to the partonic threshold up to NNLL was considered in [26–32]. The mixed QCD+EW corrections were calculated in [33] and the NLO QCD corrections in the Standard Model Effective Field Theory were presented in [34]. Beyond all these, the next-to-next-to-leading order (NNLO) QCD corrections are the current frontier. In the NNLO corrections, in addition to the two-loop amplitudes, the higher order contributions of one-loop amplitudes in the dimensional regulator ϵ are also necessary. In [35], the $\mathcal{O}(\epsilon^1)$ contributions for both the quark-antiquark annihilation channel and the gluon fusion channel were obtained and used to extract the Infrared (IR) singularities of corresponding two-loop amplitudes. The $\mathcal{O}(\epsilon^2)$ contributions for the gluon fusion channel have recently been known in [36]. The contributions from off-diagonal partonic channels are present in [37], which turn out to be at the per-mill level. The contributions from the $q\bar{q}$ channel with closed massless and/or massive quark loops to the two-loop amplitudes were calculated numerically in [38]. In [39], the so-called soft Higgs approximation was applied to calculate the most difficult two-loop amplitudes. This approximation is valid in the limit where the momentum of the Higgs boson is small compared to other scales in the process. Such an approximation turns out to be reasonable for calculating the total cross sections, but may not be applicable to more exclusive differential cross sections. The two-loop master integrals for leading-color QCD scattering amplitudes with closed light-quark loops in $t\bar{t}H$ production were calculated in [40], while the exact calculation of the two-loop amplitudes is still beyond the reach of current methods.

In this paper, we take a kinematic limit different from that in [39]. We consider the two-loop amplitudes for $t\bar{t}H$ production in the high-energy boosted limit, where the momentum-invariants are much larger than the mass of the top quark, i.e., $|s_{ij}| \gg m_t^2$ for all external legs i and j. In this limit, a general mass-factorization formula was given in [41–44]. Using this factorization formula, our main task becomes the calculation of the two-loop massless amplitudes, where m_t and m_H are set to zero. This is much simpler than the calculation of the fully massive amplitudes, and is made possible by the recent progresses in the integration-by-parts (IBP) reduction techniques [45–51] and the results for the two-loop five-point master integrals [52–59].

The paper is organized as follows. In section 2, we give our notations and the definitions of various quantities used in our calculation. We introduce our approximate formula for the massive amplitudes in the high-energy boosted limit in section 3, and discuss the conventions for dealing with power-suppressed contributions in section 4. We then present our numeric results in section 5 and conclude in section 6. We collect some length expressions in the appendices.

2 Notations and definition

For the production of a Higgs boson associated with a top-antitop quark pair, we consider the following two partonic processes

$$q_\beta(p_1) + \bar{q}_\alpha(p_2) \to t_k(p_3) + \bar{t}_l(p_4) + H(p_5) \,, \tag{2.1}$$

$$g_a(p_1) + g_b(p_2) \to t_k(p_3) + \bar{t}_l(p_4) + H(p_5) \,, \tag{2.2}$$

where $\alpha, \beta, a, b, k, l$ are color indices and p_i the momenta of the external partons with $p_1^2 = p_2^2 = 0$, $p_3^2 = p_4^2 = m_t^2$ and $p_5^5 = m_H^2$. The kinematic variables are defined as $s_{ij} = (p_i + \sigma_{ij} p_j)^2$, where $\sigma_{ij} = +1$ if the momenta p_i and p_j are both incoming or outgoing, and $\sigma_{ij} = -1$ otherwise.

To facilitate the calculation of the amplitudes $|\mathcal{M}_{q,g}\rangle$, we decompose them in terms of color and spin (Lorentz) structures in the color $\otimes$ spin space of external partons. Note that the subscript q or g specifies the quark-antiquark annihilation channel or the gluon fusion channel, respectively. The amplitudes $|\mathcal{M}_{q,g}\rangle$ can be expanded in the strong coupling constant α_s up to NNLO as

$$|\mathcal{M}_{q,g}\rangle = 4\pi\alpha_s \left[|\mathcal{M}_{q,g}^{(0)}\rangle + \frac{\alpha_s}{4\pi} |\mathcal{M}_{q,g}^{(1)}\rangle + \left(\frac{\alpha_s}{4\pi}\right)^2 |\mathcal{M}_{q,g}^{(2)}\rangle + \mathcal{O}(\alpha_s)^3 \right]. \tag{2.3}$$

The l-loop coefficient $|\mathcal{M}_{q,g}^{(l)}\rangle$ can be further decomposed in the color $\otimes$ spin space

$$|\mathcal{M}_{q,g}^{(l)}\rangle = \sum_{I,i} c_{Ii}^{(l)q,g} |c_I^{q,g}\rangle \otimes |d_i^{q,g}\rangle, \tag{2.4}$$

where $|c_I^{q,g}\rangle$ are the orthogonal color bases for the quark-antiquark annihilation channel and the gluon fusion channel, $|d_i^{q,g}\rangle$ denote independent spin structures. We employ the color-space formalism [60, 61], and choose the color bases as

$$
\begin{aligned}
|c_1^q\rangle &= \delta_{\alpha\beta}\,\delta_{kl}\,, \quad |c_2^q\rangle = (t^a)_{\alpha\beta}\,(t^a)_{kl}\,, \\
|c_1^g\rangle &= \delta^{ab}\,\delta_{kl}\,, \quad |c_2^g\rangle = if^{abc}\,(t^c)_{kl}\,, \quad |c_3^g\rangle = d^{abc}\,(t^c)_{kl}\,.
\end{aligned} \tag{2.5}
$$

To define the spin structures $|d_i^{q,g}\rangle$, we choose the conventional dimensional regularization (CDR) scheme and assume that the external partons live in d spacetime dimensions. There are 28 independent structures in the quark-antiquark annihilation channel and 40 independent structures in the gluon fusion channel, which are given in appendix A.1.

The ultraviolet (UV) divergences in the bare amplitudes $|\mathcal{M}_{q,g}^{\mathrm{bare}}\rangle$ are renormalized according to

$$\left|\mathcal{M}_{q,g}^R(\alpha_s, g_Y, m_t, \mu, \epsilon)\right\rangle = \left(\frac{\mu^2 e^{\gamma_E}}{4\pi}\right)^{-3\epsilon/2} Z_{q,g} Z_Q \left|\mathcal{M}_{q,g}^{\mathrm{bare}}(\alpha_s^0, g_Y^0, m_t^0, \epsilon)\right\rangle, \tag{2.6}$$

where Z_g, Z_q and Z_Q are the on-shell wave-function renormalization constants for gluons, light- and heavy-quarks, respectively. We have suppressed the dependence of the amplitudes on other kinematic variables. The Yukawa coupling g_Y is defined as

$$g_Y = \frac{e\, m_t}{2 m_W \sin(\theta_W)}. \tag{2.7}$$

We renormalize the top-quark mass in the on-shell scheme: $m_t^0 = Z_m m_t$, and the Yukawa coupling is renormalized accordingly. The strong coupling constant α_s is renormalized in the $\overline{\mathrm{MS}}$ scheme with $n_f = n_l + n_h$ active flavors. The relations between the bare couplings and the renormalized ones are given by

$$\alpha_s^0 = \left(\frac{\mu^2 e^{\gamma_E}}{4\pi}\right)^{\epsilon} Z_{\alpha_s} \alpha_s\,, \quad g_Y^0 = \left(\frac{\mu^2 e^{\gamma_E}}{4\pi}\right)^{\epsilon/2} Z_m\, g_Y\,. \tag{2.8}$$

The renormalization constants up to NNLO are given in the appendix B.

The renormalized form factors $c_{Ii}^{R;q,g}$ can be extracted as a linear combination of scalar Feynman integrals according to

$$c_{Ii}^{R;q,g} = \sum_j \frac{\left(\boldsymbol{D}_{q,g}^{-1}\right)_{ij}}{\langle c_I^{q,g}|c_I^{q,g}\rangle} \left[\langle d_j^{q,g}| \otimes \langle c_I^{q,g}|\mathcal{M}_{q,g}^R\rangle \right], \tag{2.9}$$

where $\boldsymbol{D}_{q,g}$ are matrices in the space of spin structures, whose elements are defined by $\boldsymbol{D}_{ij}^{q,g} = \langle d_i^{q,g}|d_j^{q,g}\rangle$. The polarization sum of the two initial gluons yields

$$\sum_s \varepsilon^\mu(p_1,s)\varepsilon^\nu(p_1,s) = \sum_s \varepsilon^\mu(p_2,s)\varepsilon^\nu(p_2,s) = -g^{\mu\nu} + \frac{p_1^\mu p_2^\nu + p_1^\nu p_2^\mu}{p_1 \cdot p_2}. \tag{2.10}$$

The two-loop renormalized amplitudes $|\mathcal{M}_{q,g}^{(2)R}\rangle$ are the main object of study in this work. Note that the IR singularities of $|\mathcal{M}_{q,g}^{(2)R}\rangle$ have been presented in [35]. The IR poles are obtained from the one-loop amplitude up to $\mathcal{O}(\epsilon^1)$ and a universal anomalous dimension matrix. However, for the finite part, one needs to calculate the highly non-trivial two-loop five-point Feynman integrals involving 7 physical scales. In this work, we explore the high-energy boosted limit, and use the mass-factorization [41] to approximately calculate these two-loop amplitudes.

3 Massive amplitudes in the high-energy boosted limit

3.1 The massive amplitudes from mass-factorization

Consider the amplitude for a generic $2 \to n$ partonic scattering process in QCD:

$$h_1(p_1,m_1) + h_2(p_2,m_2) \to h_3(p_3,m_3) + h_4(p_4,m_4) + \cdots + h_{n+2}(p_{n+2},m_{n+2}), \tag{3.1}$$

where m_i is the mass of the parton h_i. We work in the high-energy boosted limit, where $|s_{ij}| \gg m_k^2$ for arbitrary i,j,k and $i \neq j$. In this limit, the renormalized massive amplitude $\mathcal{M}^R$ can be factorized as [41–44]

$$\left|\mathcal{M}^R(\epsilon,\{p\},\{m\},\mu)\right\rangle = \prod_j \left(\mathcal{Z}_{[j]}^{(m|0)}(\epsilon,\{m\},\mu)\right)^{1/2}$$
$$\times \boldsymbol{S}(\epsilon,\{\tilde{p}\},\{m\},\mu) \left|\tilde{\mathcal{M}}^R(\epsilon,\{\tilde{p}\},\mu)\right\rangle + \mathcal{O}(m^2), \tag{3.2}$$

where $\tilde{\mathcal{M}}^R$ is the renormalized massless amplitude with all parton masses taken to zero. We use $\{p\}$ and $\{\tilde{p}\}$ to collectively denote the sets of all external momenta for the massive and massless amplitudes, and $\{m\}$ to denote the set of all parton masses. The $\mathcal{Z}$-factors $\mathcal{Z}_{[j]}^{(m|0)}$ and the soft function $\boldsymbol{S}$ contain all the mass logarithms $\ln(\mu^2/m^2)$, where $\boldsymbol{S}$ only receives contributions from closed-loops of massive partons starting from $\mathcal{O}(\alpha_s^2)$. The expressions of $\mathcal{Z}_{[j]}^{(m|0)}$ for gluons and quarks up to NNLO can be found in [41, 62, 63], up to terms proportional to $n_h^1 n_l^0$. These missing terms as well as the soft function can be found in [42–44]. For completeness, we give the explicit expressions in appendix C. Note that the factorization in (3.2) is correct up to power corrections of $\mathcal{O}(m^2)$. These sub-leading contributions are

currently under active investigations [64–66]. In this work, we will keep only the leading power (LP) terms and neglect the power corrections.

For the $t\bar{t}H$ production process considered in this work, there is a massive Higgs boson in the final state in addition to massive top (anti-)quarks. The Higgs boson is color neutral and is not involved in QCD interactions. We can in principle keep the Higgs mass m_H in $\tilde{\mathcal{M}}^R$ of eq. (3.2). However, since $m_H < m_t$, it is reasonable to expand in m_H as well. Therefore, for simplicity, we choose to take $m_H \to 0$ in $\tilde{\mathcal{M}}^R$. Note that this does not introduce logarithmic terms of m_H.

We are now ready to define an approximate amplitudes for $t\bar{t}H$ production in the boosted limit, given by

$$
\begin{aligned}
\left|\bar{\mathcal{M}}_{q,g}^R\left(\epsilon, \{p\}, m_t, m_H, \mu\right)\right\rangle = {} & \mathcal{Z}_{[q,g]}^{(m|0)}(\epsilon, m_t, \mu)\, \mathcal{Z}_{[t]}^{(m|0)}(\epsilon, m_t, \mu) \\
& \times \boldsymbol{\mathcal{S}}(\epsilon, \{\tilde{p}\}, m_t, \mu)\left|\tilde{\mathcal{M}}_{q,g}^R\left(\epsilon, \{\tilde{p}\}, \mu\right)\right\rangle .
\end{aligned}
\tag{3.3}
$$

The amplitude $\bar{\mathcal{M}}^R$ provides an approximation to the full amplitude $\mathcal{M}^R$ up to power corrections in m_t^2 and m_H^2. The momenta in $\tilde{\mathcal{M}}^R$ satisfy the on-shell conditions $\tilde{p}_i^2 = 0$, and we define $\tilde{s}_{ij} \equiv \sigma_{ij}\, \tilde{p}_i \cdot \tilde{p}_j$. There are some degrees of freedom in choosing how $\{\tilde{p}\}$ are related to the original momenta $\{p\}$ in the massive amplitude. We will discuss our choice in the next section. Before that, we turn to the actual calculation of the massless amplitude $\tilde{\mathcal{M}}^R$ at NNLO in the following.

3.2 Calculation of the massless amplitudes

Similar to the massive case, we renormalize the massless amplitudes according to

$$
\left|\tilde{\mathcal{M}}_{q,g}^R(\alpha_s, g_Y, \mu, \epsilon)\right\rangle = \left(\frac{\mu^2 e^{\gamma_E}}{4\pi}\right)^{-3\epsilon/2}\left|\tilde{\mathcal{M}}_{q,g}^{\text{bare}}(\alpha_s^0, g_Y^0, \epsilon)\right\rangle ,
\tag{3.4}
$$

where we have suppressed the dependence of the amplitudes on the kinematic variables. Note that the on-shell wave-function renormalization constants for gluons and quarks are always unity in the massless case. The renormalization of the strong coupling constant α_s and the Yukawa coupling constant g_Y is the same as eq. (2.8). The renormalized massless amplitudes can then be decomposed in the color $\otimes$ spin space into

$$
|\tilde{\mathcal{M}}_{q,g}^R\rangle = \sum_{I,i} \tilde{c}_{Ii}^{R;q,g}\, |c_I^{q,g}\rangle \otimes |\tilde{d}_i^{q,g}\rangle ,
\tag{3.5}
$$

where the color basis is the same as eq. (2.5). However, the number of linearly independent spin (Lorentz) structures $|\tilde{d}_i^{q,g}\rangle$ in the massless case is different from that in the massive case. There are 14 independent structures for the quark-antiquark annihilation channel and 20 independent structures for the gluon fusion channel. We list them in appendix A.2. Note that the number of massless spin structures is exactly one-half of that of massive ones. This is due to the chirality conservation of perturbative QCD vertices, which implies that the chirality flipping terms vanish when taking $m_t = 0$.

The renormalized massless form factors $\tilde{c}_{Ii}^{R;q,g}$ can be extracted according to

$$
\tilde{c}_{Ii}^{R;q,g} = \sum_j \frac{\left(\tilde{\boldsymbol{D}}_{q,g}^{-1}\right)_{ij}}{\langle c_I^{q,g}|c_I^{q,g}\rangle}\left[\langle \tilde{d}_j^{q,g}| \otimes \langle c_I^{q,g}|\tilde{\mathcal{M}}_{q,g}^R\rangle\right] ,
\tag{3.6}
$$

where $\tilde{\boldsymbol{D}}_{ij}^{q,g} = \langle \tilde{d}_i^{q,g} | \tilde{d}_j^{q,g} \rangle$. We generate the massless amplitudes using `FeynArts` [67], and manipulate the expressions with `FeynCalc` [68–70] and `FORM` [71]. After applying the projectors in eq. (3.6), the one-loop and two-loop massless form factors can be expressed as linear combinations of one-loop and two-loop scalar Feynman integrals, respectively. The two-loop scalar integrals are categorized into 180 integral families. Taking into account permutations of external momenta, there are four independent integral topologies. These integrals have been considered in refs. [52–59]. Following the notation of ref. [72], we define the two-loop integral families $G_{\tau,\sigma}$ for each topology τ in permutation σ as

$$G_{\tau,\sigma}[\vec{a}] \equiv e^{2\epsilon\gamma_E} \int \frac{d^D l_1}{\mathrm{i}\pi^{\frac{D}{2}}} \frac{d^D l_2}{\mathrm{i}\pi^{\frac{D}{2}}} \frac{1}{\vec{\boldsymbol{D}}_{\tau,\sigma}^{\vec{a}}}, \quad \vec{\boldsymbol{D}}_{\tau,\sigma}^{\vec{a}} = \prod_i D_{\tau,\sigma,i}^{a_i}. \tag{3.7}$$

For each of the four independent integral topologies, we choose the standard permutation $\sigma_0 = (1,2,3,4,5)$, and define the sets $\vec{\boldsymbol{D}}_{\tau,\sigma_0}$ as

	$\vec{D}_{a,\sigma_0}$	$\vec{D}_{b,\sigma_0}$	$\vec{D}_{c,\sigma_0}$	$\vec{D}_{d,\sigma_0}$
1	$(l_1)^2$	$(l_1)^2$	$(l_1)^2$	$(l_1)^2$
2	$(l_1+p_1)^2$	$(l_1-p_1)^2$	$(l_1-p_1)^2$	$(l_1-p_1)^2$
3	$(l_1+p_1+p_2)^2$	$(l_1-p_1-p_2)^2$	$(l_1-p_1-p_2)^2$	$(l_1-p_1-p_2)^2$
4	$(l_1-p_4-p_5)^2$	$(l_1+p_4+p_5)^2$	$(l_2)^2$	$(l_2)^2$
5	$(l_2)^2$	$(l_2)^2$	$(l_2+p_4+p_5)^2$	$(l_2+p_4+p_5)^2$
6	$(l_2-p_4-p_5)^2$	$(l_2+p_5)^2$	$(l_2+p_5)^2$	$(l_2-p_1-p_2)^2$
7	$(l_2-p_5)^2$	$(l_1-l_2)^2$	$(l_1-l_2)^2$	$(l_2+p_5)^2$
8	$(l_1-l_2)^2$	$(l_1-l_2+p_4)^2$	$(l_1-l_2+p_3)^2$	$(l_1-l_2)^2$
9	$(l_1-p_5)^2$	$(l_2-p_1)^2$	$(l_1+p_5)^2$	$(l_1-l_2+p_3)^2$
10	$(l_2+p_1)^2$	$(l_2-p_1-p_2)^2$	$(l_2-p_1)^2$	$(l_1+p_5)^2$
11	$(l_2+p_1+p_2)^2$	$(l_2+p_4+p_5)^2$	$(l_2-p_1-p_2)^2$	$(l_2-p_1)^2$

$$\tag{3.8}$$

The corresponding diagrams are depicted in figure 1.

We now need to perform IBP reduction for these four independent topologies. We note that the most difficult part is the reduction of the top-sector in topology-DP, where the total power of irreducible scalar products in the numerator can be up to 5. The IBP relations in this top-sector have been given in the literature [46–48]. For the sub-sectors in this topology, and the other three topologies, we perform IBP reduction using the program package `Kira` [73, 74] with the help of `FireFly` [75, 76]. We find that the top-sector of topology-HT is reducible and the masters in this topology can be obtained from topology-PB with a suitable permutation of external momenta. The size of these reduction relations is around 15 GB. To simplify subsequent calculations, we follow the suggestion of [46], and express the integrals in terms of the uniform transcendentality (UT) basis given in [72] for each topology.[1] The IBP coefficients are further simplified using the program package

---

[1]Note that the UT bases for the top-sector of topology-DP given in [46–48] are different from those in [72]. They are related by linear transformations.
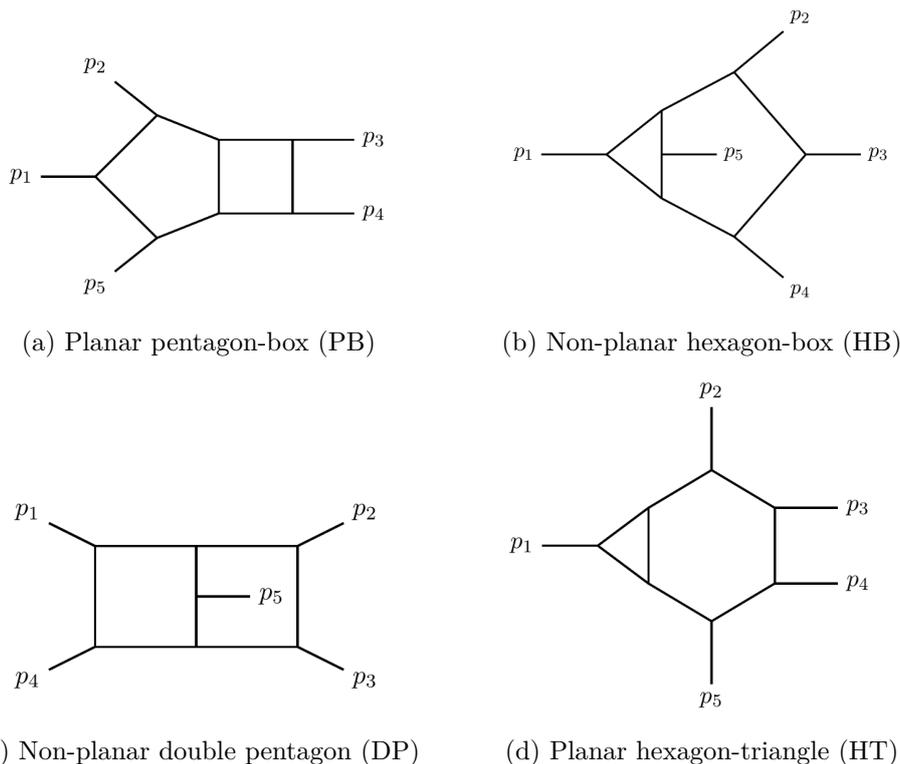
(a) Planar pentagon-box (PB)

(b) Non-planar hexagon-box (HB)

(c) Non-planar double pentagon (DP)

(d) Planar hexagon-triangle (HT)

Figure 1. Two-loop integral topologies.

MultivariateApart [51]. As a result, the size of the reduction relations becomes about 2.2 GB. Finally, the UT bases can be evaluated using the program package PentagonMI [72]. With the same program, we also compute the one-loop UT bases up to weight 4, which are necessary for calculating the one-loop form factors up to order ϵ^2.

4 Squared amplitudes and mapping between massive and massless phase-space points

We have noted in eq. (3.2) that the factorization formula receives power corrections. As such, there are ambiguities of $\mathcal{O}(m^2)$ among different conventions of using the formula. In particular, when we apply the formula to compute the physical cross sections, there are two kinds of ambiguities that we'll discuss in this section.

4.1 Squared amplitudes

The first kind of ambiguity comes from how to apply the formula to compute the squared amplitudes. Since the tree-level and one-loop massive amplitudes can be calculated exactly, the only ambiguity in the NNLO squared amplitudes lies in the interference between the two-loop amplitudes and the tree-level ones. We will pick two particular schemes and compare the outcome, while keeping in mind that other choices are possible.

The first scheme is that we strictly square the approximate amplitudes $|\bar{\mathcal{M}}_{q,g}^R\rangle$ in eq. (3.3), and extract the NNLO terms, which are simply $2\,\mathrm{Re}\,\langle\bar{\mathcal{M}}_{q,g}^{(0)R}|\bar{\mathcal{M}}_{q,g}^{(2)R}\rangle$. Here, $|\bar{\mathcal{M}}_{q,g}^{(0)R}\rangle$ are the

same as the massless tree-level amplitudes $|\tilde{\mathcal{M}}_{q,g}^{(0)R}\rangle$. The only mass information is contained in the factors of $\mathcal{Z}_{[j]}^{(m|0)}$ and the soft function $\boldsymbol{\mathcal{S}}$. We will refer to this scheme as the "massless scheme".

The second scheme is a bit more involved. We introduce a modified version of the approximate amplitudes:

$$
\begin{aligned}
\left|\hat{\mathcal{M}}_{q,g}^{R}\left(\epsilon,\{p\},m_t,m_H,\mu\right)\right\rangle = \mathcal{Z}_{[q,g]}^{(m|0)}(\epsilon,m_t,\mu)\,\mathcal{Z}_{[t]}^{(m|0)}(\epsilon,m_t,\mu) \\
\times\,\boldsymbol{\mathcal{S}}(\epsilon,\{\tilde{p}\},m_t,\mu)\sum_{I,i}\tilde{c}_{Ii}^{R;q,g}\,|c_I^{q,g}\rangle\otimes|\hat{d}_i^{q,g}\rangle
\end{aligned}
\tag{4.1}
$$

where $|\hat{d}_i^{q,g}\rangle$ are the massive version of $|\tilde{d}_i^{q,g}\rangle$. That is, the spinors and the momenta of the (anti-)top quark and the Higgs boson are treated as massive. The difference between $\hat{\mathcal{M}}_{q,g}^{R}$ and $\bar{\mathcal{M}}_{q,g}^{R}$ is power-suppressed. We can then define the interference between the approximate two-loop amplitudes with the fully massive tree-level amplitudes via $\langle\mathcal{M}_{q,g}^{(0)R}|\hat{\mathcal{M}}_{q,g}^{(2)R}\rangle$. In this setup, only the two-loop form factors $\tilde{c}_{Ii}^{(2)R;q,g}$ are purely massless and are calculated according to eq. (3.6). The other quantities, including the tree-level amplitudes $\mathcal{M}_{q,g}^{(0)R}$ and the spin (Lorentz) structures $|\hat{d}_i^{q,g}\rangle$, all contain mass information. Therefore, we will refer to this scheme as the "semi-massive scheme".

4.2 Mapping between massive and massless phase-space points

The second kind of ambiguity lies in the relation between the massive external momenta p_i and the massless external momenta $\tilde{p}_i$ in eq. (3.3). In practice, when performing phase-space integration, we first generate a set of massive momenta p_i. We then need to uniquely fix a corresponding set of $\tilde{p}_i$ that differ from p_i only by power corrections. Our convention is simple: we set the directions of the 3-momenta unchanged between p_i and $\tilde{p}_i$, and rescale the norms of the 3-momenta together with the energy parts to fulfill the massless on-shell condition while keeping momentum conservation.

To be more precise, since p_1 and p_2 are already massless, we will simply choose $\tilde{p}_1 = p_1$ and $\tilde{p}_2 = p_2$. Therefore we have $\tilde{s}_{12} = s_{12}$. We now parameterize p_i in the center-of-mass frame as

$$
\begin{aligned}
p_1 &= \frac{\sqrt{s_{12}}}{2}\left(1,0,0,1\right), \\
p_2 &= \frac{\sqrt{s_{12}}}{2}\left(1,0,0,-1\right), \\
p_3 &= \left(\sqrt{m_t^2+q_3^2},\,q_3\sin\theta_3\sin\phi_3,\,q_3\sin\theta_3\cos\phi_3,\,q_3\cos\theta_3\right), \\
p_4 &= \left(\sqrt{m_t^2+q_4^2},\,q_4\sin\theta_4\sin\phi_4,\,q_4\sin\theta_4\cos\phi_4,\,q_4\cos\theta_4\right), \\
p_5 &= \left(\sqrt{m_H^2+q_5^2},\,q_5\sin\theta_5,\,0,\,q_5\cos\theta_5\right),
\end{aligned}
\tag{4.2}
$$

where q_i is the norm of the spatial components of p_i, θ_i is the polar angle and ϕ_i is the azimuthal angle. For convenience and without loss of generality, we have set $\phi_5 = 0$. Due to momentum conservation and the on-shell conditions, there are 7 independent parameters in the right-hand side of eq. (4.2), which are chosen as s_{12}, m_t, m_H, q_5, θ_3, ϕ_3 and θ_5. Their

values satisfy the physical constraints

$$s_{12} \geq (2m_t + m_H)^2 \,, \quad 0 \leq q_5 \leq q_{5,\text{max}} = \frac{\sqrt{s_{12} - (2m_t + m_H)^2}\sqrt{s_{12} - (2m_t - m_H)^2}}{2\sqrt{s_{12}}} \,,$$

$$m_t > 0 \,, \quad m_H > 0 \,, \quad 0 \leq \theta_3 \leq \pi \,, \quad 0 \leq \phi_3 < 2\pi \,, \quad 0 \leq \theta_5 \leq \pi \,. \tag{4.3}$$

For the massless momenta $\tilde{p}_i$, we can similarly parameterize them as

$$
\begin{aligned}
\tilde{p}_1 &= \frac{\sqrt{\tilde{s}_{12}}}{2}\,(1, 0, 0, 1) \,, \\
\tilde{p}_2 &= \frac{\sqrt{\tilde{s}_{12}}}{2}\,(1, 0, 0, -1) \,, \\
\tilde{p}_3 &= \left(\tilde{q}_3, \tilde{q}_3 \sin\tilde{\theta}_3 \sin\tilde{\phi}_3, \tilde{q}_3 \sin\tilde{\theta}_3 \cos\tilde{\phi}_3, \tilde{q}_3 \cos\tilde{\theta}_3\right) \,, \\
\tilde{p}_4 &= \left(\tilde{q}_4, \tilde{q}_4 \sin\tilde{\theta}_4 \sin\tilde{\phi}_4, \tilde{q}_4 \sin\tilde{\theta}_4 \cos\tilde{\phi}_4, \tilde{q}_4 \cos\tilde{\theta}_4\right) \,, \\
\tilde{p}_5 &= \left(\tilde{q}_5, \tilde{q}_5 \sin\tilde{\theta}_5, 0, \tilde{q}_5 \cos\tilde{\theta}_5\right) \,.
\end{aligned}
\tag{4.4}
$$

As mentioned before, we will set $\tilde{s}_{12} = s_{12}$, $\tilde{\theta}_i = \theta_i$ and $\tilde{\phi}_i = \phi_i$. The remaining parameters $\tilde{q}_i$ can then be solved from momentum conservation. They can be written as

$$
\begin{aligned}
\tilde{q}_3 &= \frac{\sqrt{s_{12}}\cos\phi_4 \sin\theta_5 \sin\theta_4}{\cos\phi_4 \sin\theta_4(\sin\theta_5 - \sin\theta_3 \sin\phi_3) - \cos\phi_3 \sin\theta_3(\sin\theta_5 - \sin\theta_4 \sin\phi_4)} \,, \\
\tilde{q}_4 &= \frac{-\sqrt{s_{12}}\cos\phi_3 \sin\theta_5 \sin\theta_3}{\cos\phi_4 \sin\theta_4(\sin\theta_5 - \sin\theta_3 \sin\phi_3) - \cos\phi_3 \sin\theta_3(\sin\theta_5 - \sin\theta_4 \sin\phi_4)} \,, \\
\tilde{q}_5 &= \frac{-\sqrt{s_{12}}\sin\theta_3 \sin\theta_4 \sin(\phi_3 - \phi_4)}{\cos\phi_4 \sin\theta_4(\sin\theta_5 - \sin\theta_3 \sin\phi_3) - \cos\phi_3 \sin\theta_3(\sin\theta_5 - \sin\theta_4 \sin\phi_4)} \,.
\end{aligned}
$$

5 Numeric results

We are now ready to present the numeric results for the two-loop amplitudes based on our approximate formula. Before that, we briefly discuss the choice of the renormalization scale μ. The kinematic configuration that we're considering involves vastly different scales $|s_{ij}| \gg m_t^2$. In this case, there will be large logarithms such as $\ln(s_{ij}/m_t^2)$ no matter what we choose as μ. The standard way to deal with this problem is to resum these logarithms using renormalization group equations, based on the factorization formula (3.2) (see, e.g., [77–81]). However, in this work we are only using the factorization formula to provide an approximation of the two-loop amplitudes. Therefore, we are free to use any scale μ to present our results. We will by default set $\mu = m_t$ in the following, and will compare with other scale choices. For the other input parameters, we set $m_t = 173\,\text{GeV}$ and $m_H = 125\,\text{GeV}$.

In order to assess the validity of the approximate formula, we will first compare the approximate results with the exact ones. These exact results include the NLO squared amplitudes up to the finite parts, and the IR poles of the NNLO squared amplitudes [35]. The NLO squared amplitudes come from the interference between tree-level and one-loop amplitudes, which can be obtained from the literature as well as various program packages [10–15, 82–90]. Since we want to compare at the level of different color structures, we have recomputed the exact NLO results. The NNLO squared amplitudes receive two
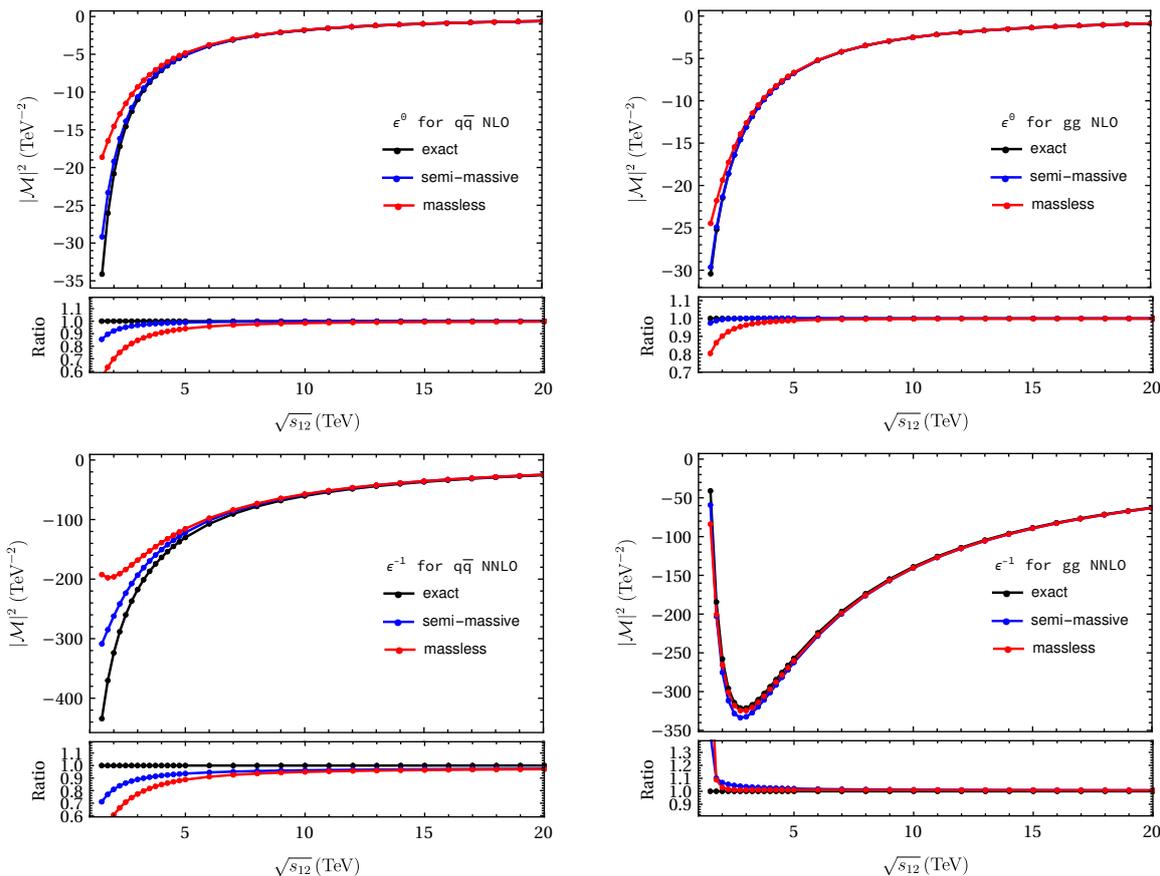
Figure 2. The squared amplitudes at $\mathcal{O}(\epsilon^0)$ for NLO and $\mathcal{O}(\epsilon^{-1})$ for NNLO in both the $q\bar{q}$ and gg channels, as a function of the partonic center-of-mass energy $\sqrt{s_{12}}$. The other kinematic variables are chosen as $\theta_3 = 14\pi/29$, $\phi_3 = 34\pi/29$, $\theta_5 = 15\pi/29$ and $q_5 = 20\,q_{5,\max}/29$. We have included the spin- and color-average factors of $1/36$ for the $q\bar{q}$ channel and $1/256$ for the gg channel. The lower panel in each plot shows the ratios between the approximate results and the exact ones.

contributions: the one-loop-squared amplitudes, and the interference between tree-level and two-loop amplitudes. The finite part of the latter contribution is the genuinely new result of this work. Hence, for convenience, we will drop the one-loop-squared amplitudes and only compare the interference terms.

We first show in figure 2 the numeric results at $\mathcal{O}(\epsilon^0)$ for NLO (upper plots) and $\mathcal{O}(\epsilon^{-1})$ for NNLO (lower plots) squared amplitudes for both $q\bar{q}$ (left plots) and gg (right plots) channels. We change the partonic center-of-mass energy $\sqrt{s_{12}}$ from about $1.5\,\mathrm{TeV}$ to $20\,\mathrm{TeV}$, and fix the other kinematic variables as $\theta_3 = 14\pi/29$, $\phi_3 = 34\pi/29$, $\theta_5 = 15\pi/29$ and $q_5 = 20\,q_{5,\max}/29$. The black lines are exact results, while the red and blue curves are approximate results using the two different schemes discussed in section 4. As expected, the approximation works better towards higher energies both at NLO and NNLO. We observe that the semi-massive scheme (the blue curves) generally has a better performance than the massless scheme. Such an effect can be attributed to the fact that the semi-massive scheme incorporates some of the power-suppressed contributions. However, this should be
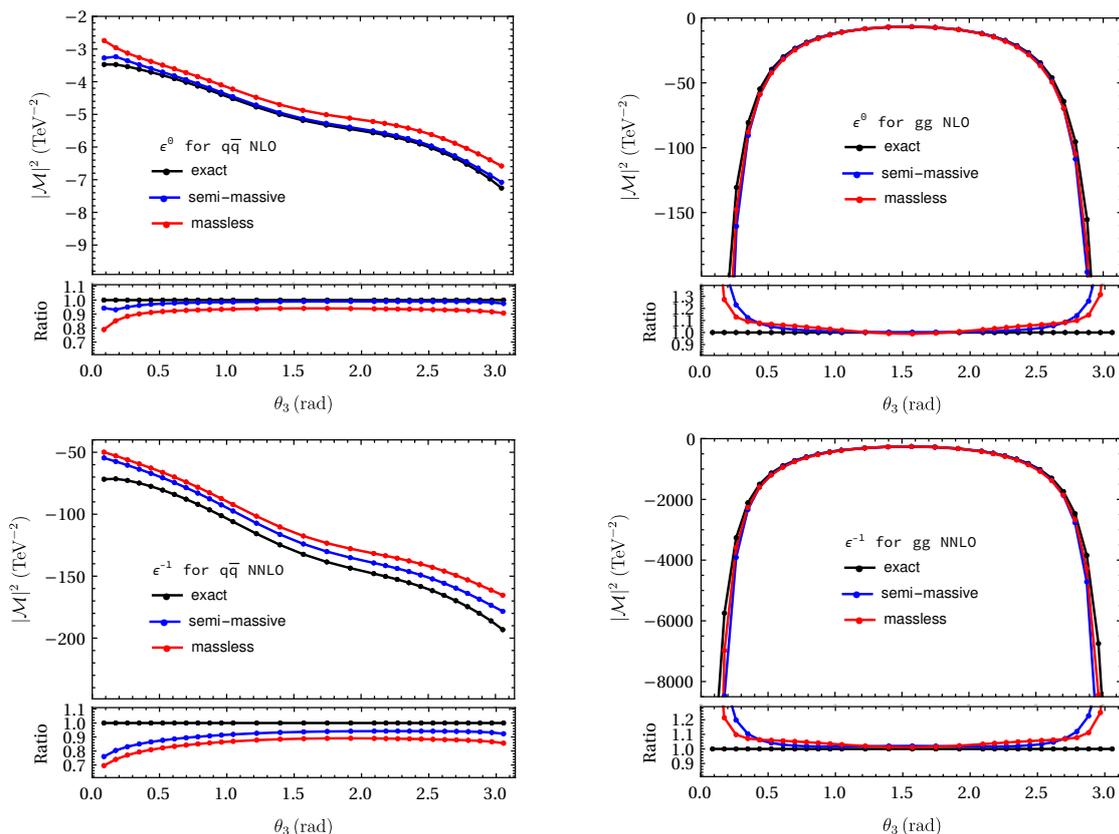
Figure 3. The squared amplitudes at $\mathcal{O}(\epsilon^0)$ for NLO and $\mathcal{O}(\epsilon^{-1})$ for NNLO in both the $q\bar{q}$ and gg channels, as a function of the angle parameter θ_3. The other kinematic variables are chosen as $\sqrt{s_{12}} = 5\,\text{TeV}$, $\phi_3 = 34\pi/29$, $\theta_5 = 15\pi/29$ and $q_5 = 20\,q_{5,\text{max}}/29$.

taken with a grain of salt since these beyond-LP terms can only be reliably obtained by a real calculation at the corresponding orders. Overall, the semi-massive scheme provides a reasonable approximation to the exact results down to $\sqrt{s_{12}} \sim 2\,\text{TeV}$ in all cases.

Interestingly, we observed from figure 2 that the approximation works better in the gg channel than in the $q\bar{q}$ one. In particular, the relative difference in the $q\bar{q}$ channel between the result in the massless scheme and the exact one is much bigger than the naive estimation of the order $(m_t^2, m_H^2)/|s_{ij}|$. In fact, this effect is already present at LO, and is inherited to higher orders. The tree-level squared amplitude in the $q\bar{q}$ channel is a rational function of m_t, m_H and s_{ij}. When expanded in the small-mass limit, there is an accidental cancellation at the LP. Numerically, the LP contribution is similar to the next-to-leading power (NLP) one. These power corrections at LO are dropped in the massless scheme, but are kept in the semi-massive scheme. This is the reason why the semi-massive scheme works much better than the massless scheme in the $q\bar{q}$ channel.

We now turn to investigate the behaviors of the approximate results when varying the angle θ_3 between $\vec{p}_3$ (of the top quark) and $\vec{p}_1$. The other parameters are fixed to be $\sqrt{s_{12}} = 5\,\text{TeV}$, $\phi_3 = 34\pi/29$, $\theta_5 = 15\pi/29$ and $q_5 = 20\,q_{5,\text{max}}/29$. It can be expected that when $\theta_3 \to 0$ or π, the approximation will become worse due to the smallness of either
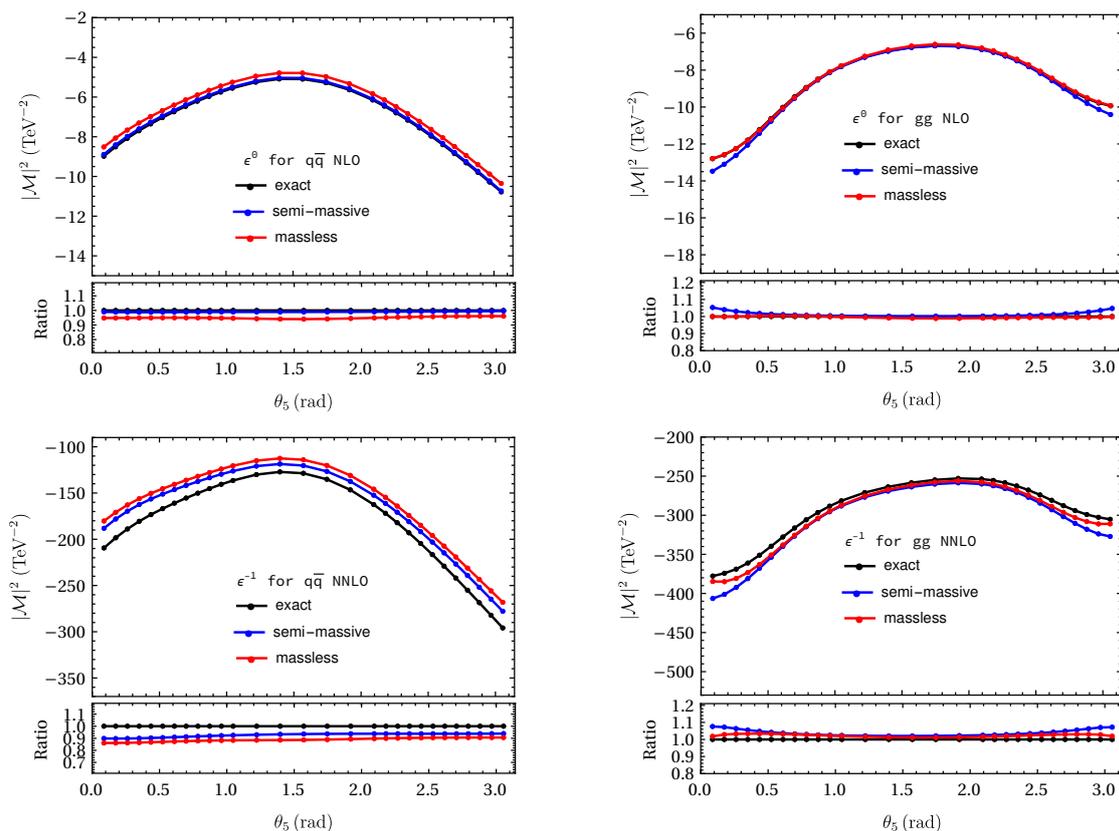
Figure 4. The squared amplitudes as a function of the angle parameter θ_5. The other kinematic variables are chosen as: $\sqrt{s_{12}} = 5\,\text{TeV}$, $\theta_3 = 14\pi/29$, $\phi_3 = 34\pi/29$ and $q_5 = 20\,q_{5,\max}/29$.

$|s_{13}|$ or $|s_{23}|$. Indeed, as is evident from figure 3, the approximate results deviate from the exact ones at the two ends of the spectrum. Especially in the gg channel, the tree-level amplitudes contain $1/(s_{13} - m_t^2)$ and $1/(s_{23} - m_t^2)$ propagators. Whether or not one takes $m_t \to 0$ will make a huge difference for these terms. This explains the wild behaviors of the blue and red curves for the gg channel at the left and right ends. Nevertheless, the semi-massive scheme still provides a reasonable approximation in a large portion of the phase space in both the $q\bar{q}$ and gg cases.

The situation is slightly different in the case of θ_5, the angle between $\vec{p}_5$ (of the Higgs boson) and $\vec{p}_1$. Since the Higgs boson is color neutral, it is expected that the QCD corrections should have a mild dependence on its momentum. This can be seen from figure 4. The approximation is rather good in the whole range of θ_5, as long as θ_3 is in the wide-angle region. From this and the previous plots, we find that the semi-massive scheme has an overall better performance than the massless scheme. Therefore, we will use the semi-massive scheme as the default to present our numerical results in the following.

Now we turn to consider the NLO and NNLO squared amplitudes at different orders in ϵ in the semi-massive scheme. We define the following ratios between the approximate
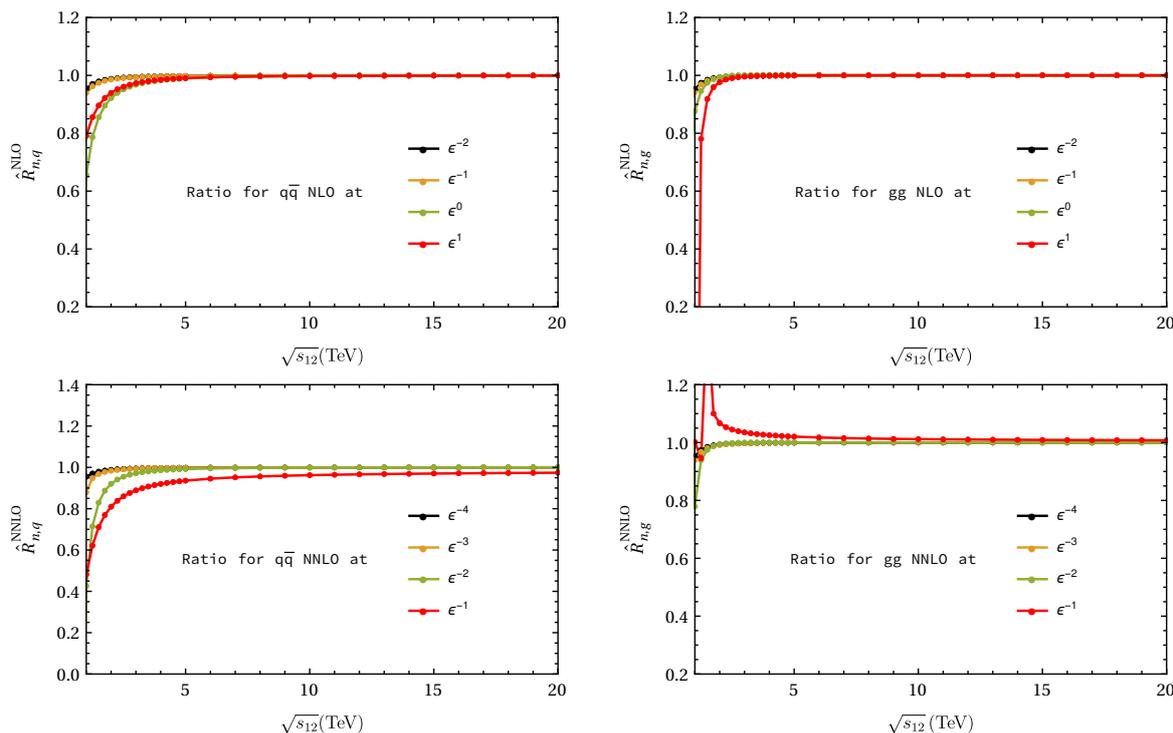
Figure 5. The ratios between the approximate results in the semi-massive scheme and the exact ones at different orders in ϵ, as functions of $\sqrt{s_{12}}$. The phase-space parameters are the same as those in the figure 2.

results and the exact ones at each order in ϵ:

$$
\hat{R}_{n,q/g}^{\mathrm{NLO}} = \frac{\mathrm{Re}\,\langle\mathcal{M}_{q/g}^{(0)R}|\hat{\mathcal{M}}_{q/g}^{(1)R}\rangle\big|_{\epsilon^n}}{\mathrm{Re}\,\langle\mathcal{M}_{q/g}^{(0)R}|\mathcal{M}_{q/g}^{(1)R}\rangle\big|_{\epsilon^n}}\,, \quad \hat{R}_{n,q/g}^{\mathrm{NNLO}} = \frac{\mathrm{Re}\,\langle\mathcal{M}_{q/g}^{(0)R}|\hat{\mathcal{M}}_{q/g}^{(2)R}\rangle\big|_{\epsilon^n}}{\mathrm{Re}\,\langle\mathcal{M}_{q/g}^{(0)R}|\mathcal{M}_{q/g}^{(2)R}\rangle\big|_{\epsilon^n}}\,, \tag{5.1}
$$

where $|\hat{\mathcal{M}}_{q/g}^{(i)R}\rangle$ are defined in eq. (4.1) and $|\mathcal{M}_{q/g}^{(i)R}\rangle$ are the exact massive amplitudes. Note that $|\mathcal{M}_{q/g}^{(1)R}\rangle$ are known up to ϵ^1 and $|\mathcal{M}_{q/g}^{(2)R}\rangle$ are known up to ϵ^{-1} in [35]. We show $\hat{R}_{n,q/g}^{\mathrm{NLO}}$ and $\hat{R}_{n,q/g}^{\mathrm{NNLO}}$ as functions of $\sqrt{s_{12}}$ in figure 5 with the same choices of phase-space parameters as in figure 2. It can be seen that, in general, the approximation works better for the coefficients of higher poles than those of lower ones. This can be expected since the higher poles are generically related to lower order (in α_s) amplitudes and anomalous dimensions. In figure 6, we show $\hat{R}_{n,q,g}^{\mathrm{NLO}}$ and $\hat{R}_{n,q,g}^{\mathrm{NNLO}}$ as functions of θ_3, with the same phase-space points as figure 3. We observe that the approximation is rather good for most values of θ_3 in the $q\bar{q}$ region except when $\theta_3 \to 0$, where the $1/\epsilon$ term at NLO and the $1/\epsilon^3$ term at NNLO behave weirdly. This behavior is partly due to the incomplete information of the power-suppressed contributions in the semi-massive scheme, which already appears at the tree-level. In the gg channel, the approximation works perfectly in the central region, while breaking down in the forward regions $\theta_3 \to 0$ or π. This can be expected since in these regions the propagator denominator $s_{13} - m_t^2$ or $s_{23} - m_t^2$ cannot be described reliably using small-mass expansion.
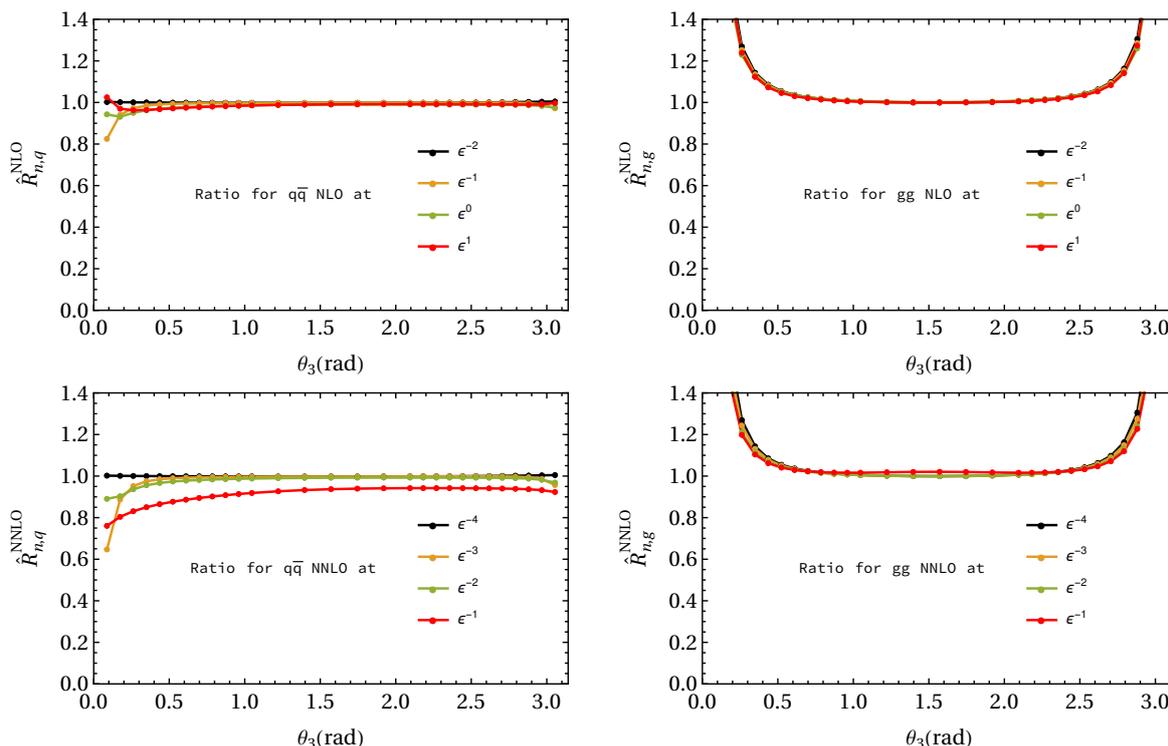
Figure 6. The ratios between the approximate results in the semi-massive scheme and the exact ones at different orders in ϵ, as functions of θ_3. The other phase-space parameters are the same as those in the figure 3.

The above results are all computed using the default scale choice $\mu = m_t$. In figure 7, we show the scale dependence of the squared amplitudes at NLO and NNLO. We can see that the quality of the approximation is nearly the same for different choices of μ. It is worth noting that without the $n_h^1 n_l^0$ terms in our factorization formula computed in [44], the approximate results would deviate for $\mu \neq m_t$. This shows that our approximate formula has correctly captured the scale-dependence of the amplitudes.

We now come to the main results of this paper, namely the approximate predictions for the finite parts of the two-loop amplitudes for $t\bar{t}H$ production. We show in figure 8 the results as functions of $\sqrt{s_{12}}$, θ_3 and θ_5, respectively. The phase-space points are chosen following figure 2, 3 and 4. Since the exact results of these finite terms are unknown, we present approximate results from both semi-massive and massless schemes for comparison. We find that the two results are quite similar at high energies, and start to deviate as we lower $\sqrt{s_{12}}$. Based on our findings in figure 2, we believe that the semi-massive scheme provides a more reliable approximation at low energies. The only exception is the $\theta_3 \to 0$ region, where the semi-massive result has a weird behavior as observed earlier in figure 6. In this region, the massless result seems to be more stable.

Besides the full squared amplitude as a whole, it is also interesting to study the squared amplitude decomposed by color coefficients. The color structure of $t\bar{t}H$ production is the same as that of $t\bar{t}$ production. Therefore, we employ the color decomposition according
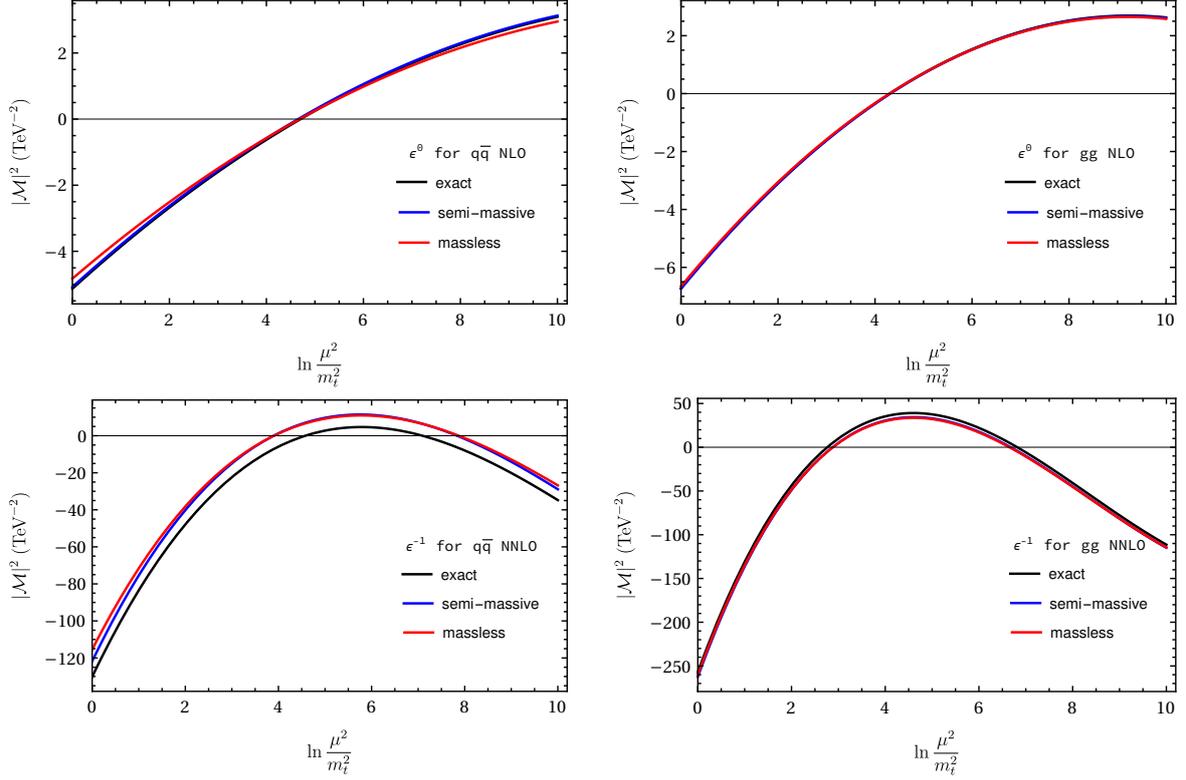
Figure 7. The squared amplitudes as a function of the renormalization scale μ. Here we show the ϵ^0 coefficients at NLO and the ϵ^{-1} coefficients at NNLO. The center-of-mass energy is chosen as $\sqrt{s_{12}} = 5\,\text{TeV}$ and other phase-space parameters are the same as those in figure 2.

to [62, 63, 91]:

$$2\,\mathrm{Re}\left\langle \mathcal{M}_q^{(0)} \middle| \mathcal{M}_q^{(2)} \right\rangle = 2(N^2-1)\left(N^2 A^q + B^q + \frac{1}{N^2}\, C^q + N n_l\, D_l^q + N n_h\, D_h^q \right.$$
$$\left. + \frac{n_l}{N}\, E_l^q + \frac{n_h}{N}\, E_h^q + n_l^2 F_l^q + n_l n_h F_{lh}^q + n_h^2 F_h^q \right),$$

$$2\,\mathrm{Re}\left\langle \mathcal{M}_g^{(0)} \middle| \mathcal{M}_g^{(2)} \right\rangle = (N^2-1)\left(N^3 A^g + N B^g + \frac{1}{N}\, C^g + \frac{1}{N^3}\, D^g \right.$$
$$+ N^2 n_l\, E_l^g + N^2 n_h\, E_h^g + n_l\, F_l^g + n_h\, F_h^g + \frac{n_l}{N^2}\, G_l^g + \frac{n_h}{N^2}\, G_h^g$$
$$\left. + N n_l^2 H_l^g + N n_l n_h H_{lh}^g + N n_h^2 H_h^g + \frac{n_l^2}{N}\, I_l^g + \frac{n_l n_h}{N}\, I_{lh}^g + \frac{n_h^2}{N}\, I_h^g \right). \tag{5.2}$$

In tables 1, 2, 3, 4, 5 and 6, we list the numeric values of the color-decomposed two-loop squared amplitudes at different orders in ϵ. We show results at three representative phase-space points, characterized by the center-of-mass energy: relatively low, intermediate and very high. These data may serve as a cross-check for an exact evaluation of the two-loop squared amplitudes in the future. Note that the numerical results of D^q, E^q and F^q were calculated recently in [38]. It will be interesting to compare their results with ours. However, the three phase-space points given in [38] are all in the low energy region ($\sqrt{s_{12}} \lesssim 1.1\,\text{TeV}$)
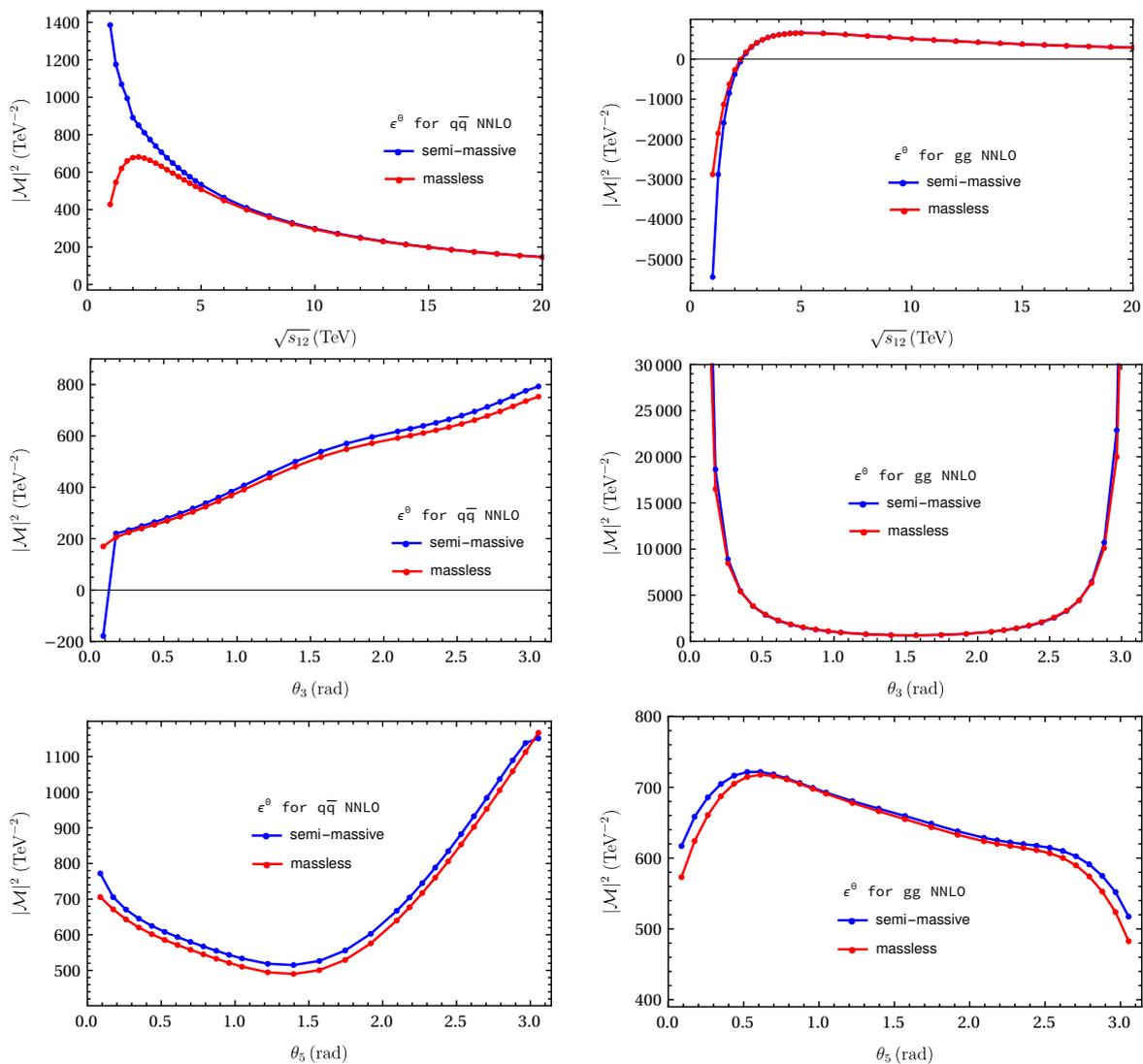
Figure 8. The finite parts of the NNLO squared amplitudes in the $q\bar{q}$ and gg channels. The phase-space points follow those in figure 2, 3 and 4.

where our high-energy boosted limit does not work very well. Therefore, we leave this comparison for future investigation.

exact / semi-	ϵ^{-4}	ϵ^{-3}	ϵ^{-2}	ϵ^{-1}	ϵ^0
A^q	0.3557588	-2.232234	18.09587	-103.9532	
	0.3515265	-2.195621	16.85573	-96.44254	348.5042
B^q	-0.7115176	7.063085	-39.95150	64.86504	
	-0.7030530	6.967777	-37.89494	130.9224	-151.0649
C^q	0.3557588	-4.830851	9.261042	84.82862	
	0.3515265	-4.772156	8.634749	83.19236	-582.0071
D_l^q		-0.3557588	0.4713803	6.932929	
		-0.3515265	0.4624203	6.840171	-43.36795
D_h^q			-1.217990	8.594097	
			-1.513230	11.12860	-48.44219
E_l^q		0.3557588	-0.6853616	1.779527	
		0.3515265	-0.6768002	1.754250	-64.57500
E_h^q			1.217990	-0.5594025	
			1.513230	-3.261069	-57.86518
F_l^q					
					0.1730958
F_{lh}^q					
					0.3461917
F_h^q					
					0.1730958
Total	1.124373	-8.136548	56.27591	-323.8812	
	1.110997	-8.004476	51.79516	-262.2186	890.7902
Ratio	0.9881	0.9838	0.9204	0.8096	

Table 1. Color-decomposed NNLO squared amplitude in the $q\bar{q}$ channel at the phase-space point $(\sqrt{s_{12}}, \sqrt{|s_{13}|}, \sqrt{|s_{14}|}, \sqrt{|s_{23}|}, \sqrt{|s_{24}|}) = (2.0000, 1.1041, 1.1373, 1.1648, 1.1402)\,\text{TeV}$, $m_t = 173\,\text{GeV}$, and $m_H = 125\,\text{GeV}$.

exact / semi-	ϵ^{-4}	ϵ^{-3}	ϵ^{-2}	ϵ^{-1}	ϵ^{0}
A^g	6.189970	-38.61149	185.2507	-502.3539	
	6.140920	-38.20303	180.8479	-466.0329	277.4175
B^g	-9.662043	67.19163	-504.2190	2664.419	
	-9.528888	66.04951	-485.4858	2302.867	-8009.039
C^g		-26.39205	137.5097	122.6492	
		-26.08095	129.1071	-282.4970	-363.2452
D^g			5.872808	-190.6910	
			5.665436	-179.9663	1016.432
E^g_l		-7.221632	30.41847	-83.58398	
		-7.164407	30.11041	-81.90409	122.4383
E^g_h			-7.090949	55.10048	
			-0.2277007	7.477590	-38.94969
F^g_l		11.27238	-51.40444	145.7744	
		11.11704	-50.54900	139.8451	-187.9518
F^g_h			13.78273	-106.0896	
				-10.76121	124.8742
G^g_l			13.19603	-19.72861	
			13.04047	-17.39200	-19.68276
G^g_h				18.82390	
					-16.44998
H^g_l			1.375549	-1.554947	
			1.364649	-1.537369	1.772607
H^g_{lh}				2.363650	
				0.07590022	-1.707018
H^g_h					
					0.2450480
I^g_l			-2.147121	2.581333	
			-2.117531	2.532773	-2.311413
I^g_{lh}				-4.594245	
					3.483198
I^g_h					
Total	4.316971	-34.94825	146.5483	-257.9766	
	4.288068	-34.65125	145.6813	-275.2426	-381.0666
Ratio	0.9933	0.9915	0.9941	1.067	

Table 2. Color-decomposed NNLO squared amplitude in the gg channel at the phase-space point $(\sqrt{s_{12}}, \sqrt{|s_{13}|}, \sqrt{|s_{14}|}, \sqrt{|s_{23}|}, \sqrt{|s_{24}|}) = (2.0000, 1.1041, 1.1373, 1.1648, 1.1402)\,\text{TeV}$, $m_t = 173\,\text{GeV}$, and $m_H = 125\,\text{GeV}$.

exact semi-	ϵ^{-4}	ϵ^{-3}	ϵ^{-2}	ϵ^{-1}	ϵ^0
A^q	0.04359554	−0.4543021	4.245433	−28.83733	
	0.04352110	−0.4519036	4.179582	−28.25268	129.5765
B^q	−0.08719108	0.9328190	−5.000430	−4.059032	
	−0.08704220	0.9261112	−4.849566	10.38085	41.35127
C^q	0.04359554	−0.4785169	−1.094868	26.09443	
	0.04352110	−0.4742076	−1.175457	26.74820	−129.2190
D_l^q		−0.04359554	0.01748520	2.409230	
		−0.04352110	0.01691567	2.401585	−21.19547
D_h^q			−0.2852286	3.073465	
			−0.2936883	3.172621	−22.32761
E_l^q		0.04359554	0.05436836	−0.7929464	
		0.04352110	0.05543837	−0.7840151	−11.00616
E_h^q			0.2852286	−1.225414	
			0.2936883	−1.294804	−10.45089
F_l^q					
					0.6690317
F_{lh}^q					
					1.338063
F_h^q					
					0.6690317
Total	0.1377834	−1.684597	14.52404	−96.47415	
	0.1375482	−1.677330	14.31068	−87.60797	360.2332
Ratio	0.9983	0.9957	0.9853	0.9081	

Table 3. Color-decomposed NNLO squared amplitude in the $q\bar{q}$ channel at the phase-space point $(\sqrt{s_{12}}, \sqrt{|s_{13}|}, \sqrt{|s_{14}|}, \sqrt{|s_{23}|}, \sqrt{|s_{24}|}) = (5.0000, 1.6558, 3.6246, 3.5411, 2.0659)\,\text{TeV}$, $m_t = 173\,\text{GeV}$, and $m_H = 125\,\text{GeV}$.

exact / semi-	ϵ^{-4}	ϵ^{-3}	ϵ^{-2}	ϵ^{-1}	ϵ^{0}
A^g	2.108278	−22.43687	154.7362	−696.5291	
	2.132335	−22.66071	156.2918	−701.0229	2001.209
B^g	−2.321466	33.50440	−283.5492	1587.447	
	−2.340932	33.78268	−286.0874	1576.900	−5796.564
C^g		−10.58208	103.5865	−310.1786	
		−10.67370	104.9121	−522.7946	1340.553
D^g			−6.330904	8.141297	
			−6.390913	9.683863	154.2983
E^g_l		−2.459657	15.63943	−54.30544	
		−2.487724	15.81008	−54.94143	95.49227
E^g_h			−0.4536370	6.220529	
			−0.09288271	3.065970	−38.53754
F^g_l		2.708377	−21.71698	76.36459	
		2.731087	−21.90274	77.13346	−130.1723
F^g_h			0.7115711	−9.676640	
				−2.778873	60.58957
G^g_l			5.291039	−17.18699	
			5.336849	−17.51022	18.44228
G^g_h				1.621799	
					−12.54769
H^g_l			0.4685062	−0.7416234	
			0.4738522	−0.7528461	0.7176704
H^g_{lh}				0.1512123	
				0.03096090	−0.5283240
H^g_h					
					0.1612425
I^g_l			−0.5158813	0.8488621	
			−0.5202071	0.8576413	−0.6890958
I^g_{lh}				−0.2371904	
					0.8557063
I^g_h					
Total	1.561222	−18.93601	124.5975	−506.8341	
	1.579695	−19.13566	125.9882	−515.3526	1265.827
Ratio	1.012	1.011	1.011	1.017	

Table 4. Color-decomposed NNLO squared amplitude in the gg channel at the phase-space point $(\sqrt{s_{12}}, \sqrt{|s_{13}|}, \sqrt{|s_{14}|}, \sqrt{|s_{23}|}, \sqrt{|s_{24}|}) = (5.0000, 1.6558, 3.6246, 3.5411, 2.0659)$ TeV, $m_t = 173$ GeV, and $m_H = 125$ GeV.

exact / semi-	ϵ^{-4}	ϵ^{-3}	ϵ^{-2}	ϵ^{-1}	ϵ^0
A^q	0.01036634	-0.1657161	1.867325	-14.63674	
	0.01036192	-0.1655484	1.862399	-14.58049	77.26753
B^q	-0.02073268	0.3368775	-2.685072	6.796855	
	-0.02072384	0.3364287	-2.674131	11.54460	-14.12207
C^q	0.01036634	-0.1711614	0.3780909	5.791447	
	0.01036192	-0.1708803	0.3723369	5.854854	-49.48764
D_l^q		-0.01036634	0.004553374	1.032195	
		-0.01036192	0.004519188	1.031455	-10.54324
D_h^q			-0.08854632	1.279040	
			-0.08907700	1.287382	-10.97078
E_l^q		0.01036634	0.01263650	-0.6003433	
		0.01036192	0.01270037	-0.5994460	-0.6874765
E_h^q			0.08854632	-0.7862173	
			0.08907700	-0.7926235	-0.3985877
F_l^q					
					0.2919736
F_{lh}^q					
					0.5839472
F_h^q					
					0.2919736
Total	0.03276276	-0.5830237	6.229379	-47.21463	
	0.03274878	-0.5825123	6.213445	-44.87048	219.5371
Ratio	0.9996	0.9991	0.9974	0.9504	

Table 5. Color-decomposed NNLO squared amplitude in the $q\bar{q}$ channel at the phase-space point $(\sqrt{s_{12}}, \sqrt{|s_{13}|}, \sqrt{|s_{14}|}, \sqrt{|s_{23}|}, \sqrt{|s_{24}|}) = (10.000, 3.3073, 7.2580, 7.0877, 4.1365)\,\mathrm{TeV}$, $m_t = 173\,\mathrm{GeV}$, and $m_H = 125\,\mathrm{GeV}$.

exact / semi-	ϵ^{-4}	ϵ^{-3}	ϵ^{-2}	ϵ^{-1}	ϵ^{0}
A^g	0.5428451	−8.014744	70.73525	−409.1486	
	0.5444174	−8.035900	70.93871	−410.1906	1595.269
B^g	−0.5947800	11.80785	−122.2304	816.5623	
	−0.5960768	11.83389	−122.5573	812.4284	−3618.243
C^g		−3.535467	46.32135	−235.2084	
		−3.543373	46.48641	−306.0970	1153.332
D^g			−3.786279	20.42499	
			−3.795128	20.68441	−16.55695
E^g_l		−0.6333192	5.140016	−20.91982	
		−0.6351536	5.154407	−20.98816	40.29084
E^g_h			−0.05982249	1.273500	
			−0.02446752	0.8755931	−18.82327
F^g_l		0.6939100	−7.171378	29.55495	
		0.6954229	−7.187486	29.64513	−56.16316
F^g_h			0.07058572	−1.610635	
				−0.7263948	27.30988
G^g_l			1.767734	−7.027765	
			1.771687	−7.066248	10.48010
G^g_h				0.2097864	
					−5.628954
H^g_l			0.1206322	−0.1890601	
			0.1209816	−0.1897854	0.1810913
H^g_{lh}				0.01994083	
				0.008155841	−0.1244663
H^g_h					
					0.05258422
I^g_l			−0.1321733	0.2159630	
			−0.1324615	0.2165426	−0.1742280
I^g_{lh}				−0.02352857	
					0.2178904
I^g_h					
Total	0.4022649	−6.474464	55.07390	−296.0855	
	0.4034700	−6.492298	55.24290	−298.2640	1062.735
Ratio	1.003	1.003	1.003	1.007	

Table 6. Color-decomposed NNLO squared amplitude in the gg channel at the phase-space point $(\sqrt{s_{12}}, \sqrt{|s_{13}|}, \sqrt{|s_{14}|}, \sqrt{|s_{23}|}, \sqrt{|s_{24}|}) = (10.000, 3.3073, 7.2580, 7.0877, 4.1365)$ TeV, $m_t = 173$ GeV, and $m_H = 125$ GeV.

6 Conclusion

In this paper, we calculate the two-loop amplitudes for $t\bar{t}H$ production at hadron colliders in the high-energy boosted limit, where the scalar products of external momenta are much larger than the top-quark mass. We employ the factorization formula recently obtained in [44], that incorporates all two-loop contributions including those proportional to the number of heavy flavors n_h. Using this factorization formula, we write the massive amplitudes as a product of the corresponding massless ones with universal factors capturing collinear and soft dynamics. We compute the massless amplitudes by IBP reduction and the existing results for the master integrals. The massive amplitudes are then computed in two schemes: the massless scheme where all the external spinors are treated as massless, and the semi-massive scheme where the external spinors are taken to be massive. For the IR poles, we compare the approximate results in the two schemes with the exact results of [35]. We find that the semi-massive scheme provides a better approximation in most of the phase-space regions. We also show that our approximation correctly reproduces the scale-dependence of the exact results. We then give our predictions for the finite parts of the two-loop squared amplitudes, which are the main new results of this work.

By combining the contributions from real emissions (including the double-real and real-virtual diagrams), our results can be utilized to compute the NNLO differential cross sections for this important process in the high-energy boosted limit. One may further incorporate the low-energy approximations such as the threshold approximation and the soft-Higgs approximation, and interpolates into the intermediate regions. This can lead to a reasonable approximation across the whole phase space, and give reliable predictions for differential cross sections from low to high energies.

Finally, it will be beneficial to provide our code in an appropriate form. At the moment this is not practical since the size of the files is rather large, and the code for the evaluation is not optimized enough to run efficiently. We are in the progress of improving these aspects of our code and will release it publicly in the near future.

A Spin (Lorentz) structures

A.1 Massive spin (Lorentz) structures

For the massive $q\bar{q}$ channel, we define $|d_i^q\rangle$ in the following form:

$$|d_i^q\rangle = \bar{v}(p_2)\,\Gamma_i\,u(p_1)\,v(p_3)\,\Gamma_i'\,\bar{u}(p_4) \quad \Rightarrow \quad \mathcal{S}_i^q = \Gamma_i \otimes \Gamma_i'\,, \tag{A.1}$$

where Γ_i denotes a string of γ matrices concerning the initial state fermion line, while Γ_i' concerns the final state fermion line. $\mathcal{S}_i^q$ are given by

$$
\begin{aligned}
&\mathcal{S}_1^q = \gamma^\mu \otimes \gamma^\mu\,, && \mathcal{S}_2^q = \gamma^\mu \otimes \gamma^\mu \slashed{p}_1\,, \\
&\mathcal{S}_3^q = \gamma^\mu \otimes \gamma^\mu \slashed{p}_2\,, && \mathcal{S}_4^q = \gamma^\mu \otimes \gamma^\mu \slashed{p}_1 \slashed{p}_2\,, \\
&\mathcal{S}_5^q = \gamma^\mu \slashed{p}_3 \slashed{p}_4 \otimes \gamma^\mu\,, && \mathcal{S}_6^q = \gamma^\mu \slashed{p}_3 \slashed{p}_4 \otimes \gamma^\mu \slashed{p}_1\,, \\
&\mathcal{S}_7^q = \gamma^\mu \slashed{p}_3 \slashed{p}_4 \otimes \gamma^\mu \slashed{p}_2\,, && \mathcal{S}_8^q = \gamma^\mu \slashed{p}_3 \slashed{p}_4 \otimes \gamma^\mu \slashed{p}_1 \slashed{p}_2\,, \\
&\mathcal{S}_9^q = \slashed{p}_3 \otimes \mathbf{1}\,, && \mathcal{S}_{10}^q = \slashed{p}_3 \otimes \slashed{p}_1\,, \\
&\mathcal{S}_{11}^q = \slashed{p}_3 \otimes \slashed{p}_2\,, && \mathcal{S}_{12}^q = \slashed{p}_3 \otimes \slashed{p}_1 \slashed{p}_2\,, \\
&\mathcal{S}_{13}^q = \slashed{p}_4 \otimes \mathbf{1}\,, && \mathcal{S}_{14}^q = \slashed{p}_4 \otimes \slashed{p}_1\,, \\
&\mathcal{S}_{15}^q = \slashed{p}_4 \otimes \slashed{p}_2\,, && \mathcal{S}_{16}^q = \slashed{p}_4 \otimes \slashed{p}_1 \slashed{p}_2\,, \\
&\mathcal{S}_{17}^q = \gamma^\mu \gamma^\nu \slashed{p}_3 \otimes \gamma^\mu \gamma^\nu\,, && \mathcal{S}_{18}^q = \gamma^\mu \gamma^\nu \slashed{p}_3 \otimes \gamma^\mu \gamma^\nu \slashed{p}_1\,, \\
&\mathcal{S}_{19}^q = \gamma^\mu \gamma^\nu \slashed{p}_3 \otimes \gamma^\mu \gamma^\nu \slashed{p}_2\,, && \mathcal{S}_{20}^q = \gamma^\mu \gamma^\nu \slashed{p}_3 \otimes \gamma^\mu \gamma^\nu \slashed{p}_1 \slashed{p}_2\,, \\
&\mathcal{S}_{21}^q = \gamma^\mu \gamma^\nu \slashed{p}_4 \otimes \gamma^\mu \gamma^\nu\,, && \mathcal{S}_{22}^q = \gamma^\mu \gamma^\nu \slashed{p}_4 \otimes \gamma^\mu \gamma^\nu \slashed{p}_1\,, \\
&\mathcal{S}_{23}^q = \gamma^\mu \gamma^\nu \slashed{p}_4 \otimes \gamma^\mu \gamma^\nu \slashed{p}_2\,, && \mathcal{S}_{24}^q = \gamma^\mu \gamma^\nu \slashed{p}_4 \otimes \gamma^\mu \gamma^\nu \slashed{p}_1 \slashed{p}_2\,, \\
&\mathcal{S}_{25}^q = \gamma^\mu \gamma^\nu \gamma^\rho \otimes \gamma^\mu \gamma^\nu \gamma^\rho\,, && \mathcal{S}_{26}^q = \gamma^\mu \gamma^\nu \gamma^\rho \otimes \gamma^\mu \gamma^\nu \gamma^\rho \slashed{p}_1\,, \\
&\mathcal{S}_{27}^q = \gamma^\mu \gamma^\nu \gamma^\rho \otimes \gamma^\mu \gamma^\nu \gamma^\rho \slashed{p}_2\,, && \mathcal{S}_{28}^q = \gamma^\mu \gamma^\nu \gamma^\rho \otimes \gamma^\mu \gamma^\nu \gamma^\rho \slashed{p}_1 \slashed{p}_2\,.
\end{aligned} \tag{A.2}
$$

For the massive gg channel, we define $|d_i^g\rangle$ in the following form:

$$
|d_i^g\rangle = \varepsilon_\mu\left(p_1, s\right) \varepsilon_\nu\left(p_2, s\right) v(p_3)\, \Gamma_i^{\mu\nu}\, \bar{u}(p_4)\,, \tag{A.3}
$$

where $\Gamma_i^{\mu\nu}$ are given by

$$
\begin{aligned}
&\Gamma_1^{\mu\nu} = \gamma^\mu \gamma^\nu \slashed{p}_1 \slashed{p}_2\,, && \Gamma_2^{\mu\nu} = \mathbf{1} g^{\mu\nu}\,, && \Gamma_3^{\mu\nu} = \mathbf{1} p_3^\mu p_3^\nu\,, && \Gamma_4^{\mu\nu} = \mathbf{1} p_4^\mu p_4^\nu\,, \\
&\Gamma_5^{\mu\nu} = \gamma^\mu \gamma^\nu\,, && \Gamma_6^{\mu\nu} = \slashed{p}_1 \slashed{p}_2 g^{\mu\nu}\,, && \Gamma_7^{\mu\nu} = \slashed{p}_1 \slashed{p}_2 p_3^\mu p_3^\nu\,, && \Gamma_8^{\mu\nu} = \slashed{p}_1 \slashed{p}_2 p_4^\mu p_4^\nu\,, \\
&\Gamma_9^{\mu\nu} = \gamma^\mu \gamma^\nu \slashed{p}_1\,, && \Gamma_{10}^{\mu\nu} = \gamma^\mu \slashed{p}_1 \slashed{p}_2 p_3^\nu\,, && \Gamma_{11}^{\mu\nu} = \gamma^\mu \slashed{p}_1 \slashed{p}_2 p_4^\nu\,, && \Gamma_{12}^{\mu\nu} = \gamma^\mu \slashed{p}_1 p_3^\nu\,, \\
&\Gamma_{13}^{\mu\nu} = \gamma^\mu \slashed{p}_1 p_4^\nu\,, && \Gamma_{14}^{\mu\nu} = \gamma^\mu \slashed{p}_2 p_3^\nu\,, && \Gamma_{15}^{\mu\nu} = \gamma^\mu \slashed{p}_2 p_4^\nu\,, && \Gamma_{16}^{\mu\nu} = \slashed{p}_1 \slashed{p}_2 p_3^\mu p_4^\nu\,, \\
&\Gamma_{17}^{\mu\nu} = \gamma^\mu p_3^\nu\,, && \Gamma_{18}^{\mu\nu} = \gamma^\mu p_4^\nu\,, && \Gamma_{19}^{\mu\nu} = \slashed{p}_1 g^{\mu\nu}\,, && \Gamma_{20}^{\mu\nu} = \slashed{p}_1 p_3^\mu p_3^\nu\,, \\
&\Gamma_{21}^{\mu\nu} = \slashed{p}_1 p_3^\mu p_4^\nu\,, && \Gamma_{22}^{\mu\nu} = \slashed{p}_1 p_3^\nu p_4^\mu\,, && \Gamma_{23}^{\mu\nu} = \slashed{p}_1 p_4^\mu p_4^\nu\,, && \Gamma_{24}^{\mu\nu} = \mathbf{1} p_3^\mu p_4^\nu\,, \\
&\Gamma_{25}^{\mu\nu} = \gamma^\mu \gamma^\nu \slashed{p}_2\,, && \Gamma_{26}^{\mu\nu} = \gamma^\nu \slashed{p}_1 \slashed{p}_2 p_3^\mu\,, && \Gamma_{27}^{\mu\nu} = \gamma^\nu \slashed{p}_1 \slashed{p}_2 p_4^\mu\,, && \Gamma_{28}^{\mu\nu} = \gamma^\nu \slashed{p}_2 p_3^\mu\,, \\
&\Gamma_{29}^{\mu\nu} = \gamma^\nu \slashed{p}_2 p_4^\mu\,, && \Gamma_{30}^{\mu\nu} = \gamma^\nu \slashed{p}_1 p_3^\mu\,, && \Gamma_{31}^{\mu\nu} = \gamma^\nu \slashed{p}_1 p_4^\mu\,, && \Gamma_{32}^{\mu\nu} = \slashed{p}_1 \slashed{p}_2 p_3^\nu p_4^\mu\,, \\
&\Gamma_{33}^{\mu\nu} = \gamma^\nu p_3^\mu\,, && \Gamma_{34}^{\mu\nu} = \gamma^\nu p_4^\mu\,, && \Gamma_{35}^{\mu\nu} = \slashed{p}_2 g^{\mu\nu}\,, && \Gamma_{36}^{\mu\nu} = \slashed{p}_2 p_3^\mu p_3^\nu\,, \\
&\Gamma_{37}^{\mu\nu} = \slashed{p}_2 p_3^\nu p_4^\mu\,, && \Gamma_{38}^{\mu\nu} = \slashed{p}_2 p_3^\mu p_4^\nu\,, && \Gamma_{39}^{\mu\nu} = \slashed{p}_2 p_4^\mu p_4^\nu\,, && \Gamma_{40}^{\mu\nu} = \mathbf{1} p_3^\nu p_4^\mu\,.
\end{aligned} \tag{A.4}
$$

A.2 Massless spin (Lorentz) structures

For the massless $q\bar{q}$ channel, we define $|\tilde{d}_i^q\rangle$ in the following form:

$$
|\tilde{d}_i^q\rangle = \bar{v}(\tilde{p}_2)\, \tilde{\Gamma}_i\, u(\tilde{p}_1)\, v(\tilde{p}_3)\, \tilde{\Gamma}_i'\, \bar{u}(\tilde{p}_4)\,, \quad \Rightarrow \quad \tilde{\mathcal{S}}_i^q = \tilde{\Gamma}_i \otimes \tilde{\Gamma}_i'\,, \tag{A.5}
$$

where $\tilde{\Gamma}_i$ denotes a string of γ matrices concerning the initial state fermion line, while $\tilde{\Gamma}'_i$ concerns the final state fermion line. $\tilde{\mathcal{S}}_i^q$ are given by

$$\tilde{\mathcal{S}}_1^q = \tilde{\not{p}}_3 \otimes \mathbf{1}\,, \qquad\qquad\qquad \tilde{\mathcal{S}}_2^q = \tilde{\not{p}}_4 \otimes \mathbf{1}\,,$$
$$\tilde{\mathcal{S}}_3^q = \gamma^\mu \otimes \gamma^\mu \tilde{\not{p}}_1\,, \qquad\qquad \tilde{\mathcal{S}}_4^q = \gamma^\mu \otimes \gamma^\mu \tilde{\not{p}}_2\,,$$
$$\tilde{\mathcal{S}}_5^q = \tilde{\not{p}}_3 \otimes \tilde{\not{p}}_1 \tilde{\not{p}}_2\,, \qquad\qquad \tilde{\mathcal{S}}_6^q = \tilde{\not{p}}_4 \otimes \tilde{\not{p}}_1 \tilde{\not{p}}_2\,,$$
$$\tilde{\mathcal{S}}_7^q = \gamma^\mu \gamma^\nu \tilde{\not{p}}_3 \otimes \gamma^\mu \gamma^\nu\,, \qquad\quad \tilde{\mathcal{S}}_8^q = \gamma^\mu \gamma^\nu \tilde{\not{p}}_4 \otimes \gamma^\mu \gamma^\nu\,,$$
$$\tilde{\mathcal{S}}_9^q = \gamma^\mu \tilde{\not{p}}_3 \tilde{\not{p}}_4 \otimes \gamma^\mu \tilde{\not{p}}_1\,, \qquad\quad \tilde{\mathcal{S}}_{10}^q = \gamma^\mu \tilde{\not{p}}_3 \tilde{\not{p}}_4 \otimes \gamma^\mu \tilde{\not{p}}_2\,,$$
$$\tilde{\mathcal{S}}_{11}^q = \gamma^\mu \gamma^\nu \gamma^\rho \otimes \gamma^\mu \gamma^\nu \gamma^\rho \tilde{\not{p}}_1\,, \qquad \tilde{\mathcal{S}}_{12}^q = \gamma^\mu \gamma^\nu \gamma^\rho \otimes \gamma^\mu \gamma^\nu \gamma^\rho \tilde{\not{p}}_2\,,$$
$$\tilde{\mathcal{S}}_{13}^q = \gamma^\mu \gamma^\nu \tilde{\not{p}}_3 \otimes \gamma^\mu \gamma^\nu \tilde{\not{p}}_1 \tilde{\not{p}}_2\,, \qquad \tilde{\mathcal{S}}_{14}^q = \gamma^\mu \gamma^\nu \tilde{\not{p}}_4 \otimes \gamma^\mu \gamma^\nu \tilde{\not{p}}_1 \tilde{\not{p}}_2\,. \tag{A.6}$$

For the massless gg channel, we define $|\tilde{d}_i^g\rangle$ in the following form:

$$|\tilde{d}_i^g\rangle = \varepsilon_\mu\,(\tilde{p}_1, s)\,\varepsilon_\nu\,(\tilde{p}_2, s)\,v(\tilde{p}_3)\,\tilde{\Gamma}_i^{\mu\nu}\,\bar{u}(\tilde{p}_4)\,, \tag{A.7}$$

where $\tilde{\Gamma}_i^{\mu\nu}$ are given by

$$\tilde{\Gamma}_1^{\mu\nu} = \gamma^\mu \gamma^\nu\,, \qquad \tilde{\Gamma}_2^{\mu\nu} = \gamma^\mu \gamma^\nu \tilde{\not{p}}_1 \tilde{\not{p}}_2\,, \qquad \tilde{\Gamma}_3^{\mu\nu} = \mathbf{1} g^{\mu\nu}\,, \qquad \tilde{\Gamma}_4^{\mu\nu} = \tilde{\not{p}}_1 \tilde{\not{p}}_2 g^{\mu\nu}\,,$$
$$\tilde{\Gamma}_5^{\mu\nu} = \gamma^\nu \tilde{\not{p}}_1 \tilde{p}_3^\mu\,, \qquad \tilde{\Gamma}_6^{\mu\nu} = \gamma^\nu \tilde{\not{p}}_2 \tilde{p}_3^\mu\,, \qquad \tilde{\Gamma}_7^{\mu\nu} = \gamma^\nu \tilde{\not{p}}_1 \tilde{p}_4^\mu\,, \qquad \tilde{\Gamma}_8^{\mu\nu} = \gamma^\nu \tilde{\not{p}}_2 \tilde{p}_4^\mu\,,$$
$$\tilde{\Gamma}_9^{\mu\nu} = \gamma^\mu \tilde{\not{p}}_1 \tilde{p}_3^\nu\,, \qquad \tilde{\Gamma}_{10}^{\mu\nu} = \gamma^\mu \tilde{\not{p}}_2 \tilde{p}_3^\nu\,, \qquad \tilde{\Gamma}_{11}^{\mu\nu} = \mathbf{1} \tilde{p}_3^\mu \tilde{p}_3^\nu\,, \qquad \tilde{\Gamma}_{12}^{\mu\nu} = \tilde{\not{p}}_1 \tilde{\not{p}}_2 \tilde{p}_3^\mu \tilde{p}_3^\nu\,,$$
$$\tilde{\Gamma}_{13}^{\mu\nu} = \mathbf{1} \tilde{p}_3^\nu \tilde{p}_4^\mu\,, \qquad \tilde{\Gamma}_{14}^{\mu\nu} = \tilde{\not{p}}_1 \tilde{\not{p}}_2 \tilde{p}_3^\nu \tilde{p}_4^\mu\,, \qquad \tilde{\Gamma}_{15}^{\mu\nu} = \gamma^\mu \tilde{\not{p}}_1 \tilde{p}_4^\nu\,, \qquad \tilde{\Gamma}_{16}^{\mu\nu} = \gamma^\mu \tilde{\not{p}}_2 \tilde{p}_4^\nu\,,$$
$$\tilde{\Gamma}_{17}^{\mu\nu} = \mathbf{1} \tilde{p}_3^\mu \tilde{p}_4^\nu\,, \qquad \tilde{\Gamma}_{18}^{\mu\nu} = \tilde{\not{p}}_1 \tilde{\not{p}}_2 \tilde{p}_3^\mu \tilde{p}_4^\nu\,, \qquad \tilde{\Gamma}_{19}^{\mu\nu} = \mathbf{1} \tilde{p}_4^\mu \tilde{p}_4^\nu\,, \qquad \tilde{\Gamma}_{20}^{\mu\nu} = \tilde{\not{p}}_1 \tilde{\not{p}}_2 \tilde{p}_4^\mu \tilde{p}_4^\nu\,. \tag{A.8}$$

B Renormalization constant

In this section, we present the various renormalization constants needed in our work. Up to NNLO, the renormalization constant of QCD coupling α_s is given by

$$Z_{\alpha_s} = 1 - \left(\frac{\alpha_s}{4\pi}\right)\frac{\beta_0}{\epsilon} + \left(\frac{\alpha_s}{4\pi}\right)^2 \left(\frac{\beta_0^2}{\epsilon^2} - \frac{\beta_1}{2\epsilon}\right)\,, \tag{B.1}$$

where

$$\beta_0 = \frac{11}{3}C_A - \frac{4}{3}T_F n_f\,, \quad \beta_1 = \frac{34}{3}C_A^2 - \frac{20}{3}C_A T_F n_f - 4 C_F T_F n_f\,. \tag{B.2}$$

Up to NNLO, the top-quark mass renormalization constant in the on-shell scheme is given by:

$$Z_m = 1 + \frac{\alpha_s}{4\pi} C_F \left[-\frac{3}{\epsilon} - (4 + 3L_\mu) - \epsilon \left(8 + 4L_\mu + \frac{\pi^2}{4} + \frac{3}{2}L_\mu^2\right)\right. \tag{B.3}$$

$$\left. + \epsilon^2 \left(-L_\mu \left(8 + \frac{\pi^2}{4}\right) - 2L_\mu^2 - \frac{L_\mu^3}{2} - 48 - \frac{\pi^2}{3} + \zeta_3\right)\right]$$

$$+ \left(\frac{\alpha_s}{4\pi}\right)^2 \left\{ C_A \left[\frac{11}{2\epsilon^2} - \frac{97}{12\epsilon} + \frac{4\pi^2}{3} - \frac{1111}{24} + 6\zeta_3 - \frac{11L_\mu^2}{2} - 4\pi^2 L_\mu - \frac{185L_\mu}{6}\right]\right.$$

$$+ C_F \left[\frac{9}{2\epsilon^2} + \frac{36L_\mu + 45}{4\epsilon} + \frac{1}{8}\left(-96\zeta_3 + 199 - 34\pi^2\right) + 9L_\mu^2 + 8\pi^2 L_\mu + \frac{45L_\mu}{2}\right]$$

$$+ T_F n_h \left(-\frac{2}{\epsilon^2} + \frac{5}{3\epsilon} + 2L_\mu^2 + \frac{26L_\mu}{3} - \frac{8\pi^2}{3} + \frac{143}{6}\right)$$

$$\left. + T_F n_l \left[-\frac{2}{\epsilon^2} + \frac{5}{3\epsilon} + \frac{1}{6}\left(71 + 8\pi^2\right) + 2L_\mu^2 + \frac{26L_\mu}{3}\right]\right\} + \mathcal{O}(\alpha_s^3)\,, \tag{B.4}$$

which is also used to renormalize the top-Higgs Yuakawa coupling according to eq. (2.8). The on-shell wave-function renormalization constants are

$$Z_q = 1 + \mathcal{O}(\alpha_s^2),$$

$$Z_g = 1 + \frac{\alpha_s}{4\pi} T_F n_h \left[-\frac{4}{3\epsilon} - \frac{4}{3} L_\mu - \epsilon \left(\frac{\pi^2}{9} + \frac{2}{3} L_\mu^2 \right) + \epsilon^2 \left(-\frac{\pi^2}{9} L_\mu - \frac{2}{9} L_\mu^3 + \frac{4}{9} \zeta_3 \right) \right] \quad \text{(B.5)}$$

$$+ \mathcal{O}(\alpha_s^2),$$

$$Z_Q = 1 + \frac{\alpha_s}{4\pi} C_F \left[-\frac{3}{\epsilon} - (4 + 3L_\mu) - \epsilon \left(8 + 4L_\mu + \frac{\pi^2}{4} + \frac{3}{2} L_\mu^2 \right) \right. \quad \text{(B.6)}$$

$$\left. + \epsilon^2 \left(-L_\mu \left(8 + \frac{\pi^2}{4} \right) - 2L_\mu^2 - \frac{L_\mu^3}{2} - 48 - \frac{\pi^2}{3} + \zeta_3 \right) \right] + \mathcal{O}(\alpha_s^2). \quad \text{(B.7)}$$

C Matching coefficient in mass-factorization formula

In this section, we present the soft function $\boldsymbol{S}$ and the $\mathcal{Z}$-factors $\mathcal{Z}_{[i]}^{(m|0)}$ for gluons and quarks up to NNLO, which can be expanded in strong coupling constant α_s as

$$\boldsymbol{S}(\{p\}, \{m\}, \epsilon) = 1 + \sum_{n=1}^{\infty} \left(\frac{\alpha_s}{4\pi} \right)^n \boldsymbol{S}^{(n)},$$

$$\mathcal{Z}_{[j]}^{(m|0)}(\{m\}, \epsilon) = 1 + \sum_{n=1}^{\infty} \left(\frac{\alpha_s}{4\pi} \right)^n \mathcal{Z}_{[j]}^{(n)}. \quad \text{(C.1)}$$

General results of soft function and $\mathcal{Z}$-factors can be found in [41–44, 62, 63], here we only present the results satisfied for the $t\bar{t}H$ production process. Up to the second order, the soft function is given by

$$\boldsymbol{S}(\{\tilde{p}\}, m_t) = 1 + \left(\frac{\alpha_s}{4\pi} \right)^2 \sum_{\substack{i,j \\ i \neq j}} (-\boldsymbol{T}_i \cdot \boldsymbol{T}_j) \mathcal{S}^{(2)}(\tilde{s}_{ij}, m_t^2) + \mathcal{O}(\alpha_s^3), \quad \text{(C.2)}$$

where i and j run over all colored external legs, and

$$\mathcal{S}^{(2)}(\tilde{s}_{ij}, m_t^2) = T_F \left(\frac{\mu^2}{m_t^2} \right)^{2\epsilon} \left(-\frac{4}{3\epsilon^2} + \frac{20}{9\epsilon} - \frac{112}{27} - \frac{4\zeta_2}{3} \right) \ln \frac{-\tilde{s}_{ij}}{m_t^2}. \quad \text{(C.3)}$$

The boldface $\boldsymbol{T}_i$ is the color generator for the external parton i which is an operator in the color space [60, 61]. For a final-state quark or an initial-state anti-quark, $(\boldsymbol{T}_i^a)_{\alpha\beta} = t_{\alpha\beta}^a$; for a final-state anti-quark or an initial-state quark, $(\boldsymbol{T}_i^a)_{\alpha\beta} = -t_{\beta\alpha}^a$; and for a gluon, $(\boldsymbol{T}_i^a)_{bc} = -if^{abc}$. The dot product is $\boldsymbol{T}_i \cdot \boldsymbol{T}_j \equiv \boldsymbol{T}_i^a \boldsymbol{T}_j^a$ with repeated indices summed over.

The $\mathcal{Z}$-factor for massless quarks starts at α_s^2, and is given by

$$\mathcal{Z}_{[q]}^{(2)} = C_F T_F \left(\frac{\mu^2}{m_t^2} \right)^{2\epsilon} \left[\frac{2}{\epsilon^3} + \frac{8}{9\epsilon^2} - \frac{1}{\epsilon} \left(\frac{65}{27} + \frac{2\zeta_2}{3} \right) + \frac{875}{54} + \frac{16\zeta_2}{3} - \frac{20\zeta_3}{3} \right]. \quad \text{(C.4)}$$

The $\mathcal{Z}$-factor for massive quark, i.e. top quark, starts at α_s, and the one-loop coefficient $\mathcal{Z}_{[t]}^{(1)}$ is given by

$$
\begin{aligned}
\mathcal{Z}_{[t]}^{(1)} = C_F \Bigg\{ & \frac{2}{\epsilon^2} + \frac{2L_\mu + 1}{\epsilon} + L_\mu^2 + L_\mu + 4 + \zeta_2 + \epsilon \left[\frac{L_\mu^3}{3} + \frac{L_\mu^2}{2} + (4+\zeta_2)L_\mu + 8 + \frac{\zeta_2}{2} - \frac{2\zeta_3}{3} \right] \\
& + \epsilon^2 \left[\frac{L_\mu^4}{12} + \frac{L_\mu^3}{6} + \left(2+\frac{\zeta_2}{2}\right)L_\mu^2 + \left(8 + \frac{\zeta_2}{2} - \frac{2}{3}\zeta_3\right)L_\mu + 16 + 2\zeta_2 - \frac{\zeta_3}{3} + \frac{9}{20}\zeta_2^2 \right] \Bigg\},
\end{aligned}
$$
(C.5)

where $L_\mu = \ln\left(\mu^2/m_t^2\right)$. The two-loop coefficient $\mathcal{Z}_{[t]}^{(2)}$ can be split into two parts:

$$
\mathcal{Z}_{[t]}^{(2)} = \mathcal{Z}_{[t]}^{(2),l} + \mathcal{Z}_{[t]}^{(2),t},
$$
(C.6)

where $\mathcal{Z}_{[t]}^{(2),l}$ contains contributions from gluon loops and light-quark loops; $\mathcal{Z}_{[t]}^{(2),t}$ denotes the contribution from a loop insertion of top quark itself, and they are given by

$$
\begin{aligned}
\mathcal{Z}_{[t]}^{(2),l} = & C_F^2 \frac{2}{\epsilon^4} + \frac{1}{\epsilon^3}\left[C_F^2 (4L_\mu + 2) - \frac{11}{2}C_F C_A + n_l C_F \right] + \frac{1}{\epsilon^2}\Bigg[C_F^2\Big(4L_\mu^2 + 4L_\mu + \frac{17}{2} \\
& + 2\zeta_2\Big) - C_F C_A\left(\frac{11}{3}L_\mu - \frac{17}{9} + \zeta_2\right) + n_l C_F\left(\frac{2}{3}L_\mu - \frac{2}{9}\right) \Bigg] + \frac{1}{\epsilon}\Bigg\{ C_F^2\Big[\frac{8}{3}L_\mu^3 + 4L_\mu^2 \\
& + (17 + 4\zeta_2)L_\mu + \frac{83}{4} - 4\zeta_2 + \frac{32}{3}\zeta_3\Big] + C_F C_A\Big[\left(\frac{67}{9} - 2\zeta_2\right)L_\mu + \frac{373}{108} + \frac{15}{2}\zeta_2 \\
& - 15\zeta_3\Big] + n_l C_F\left(-\frac{10}{9}L_\mu - \frac{5}{54} - \zeta_2\right)\Bigg\} + C_F^2\Big[\frac{4}{3}L_\mu^4 + \frac{8}{3}L_\mu^3 + (17 + 4\zeta_2)L_\mu^2 \\
& + \left(\frac{83}{2} - 8\zeta_2 + \frac{64}{3}\zeta_3\right)L_\mu + \frac{561}{8} + \frac{61}{2}\zeta_2 - \frac{22}{3}\zeta_3 - 48\ln 2\zeta_2 - \frac{77}{5}\zeta_2^2\Big] \\
& + C_F C_A\Big[\frac{11}{9}L_\mu^3 + \left(\frac{167}{18} - 2\zeta_2\right)L_\mu^2 + \left(\frac{1165}{54} + \frac{56}{3}\zeta_2 - 30\zeta_3\right)L_\mu + \frac{12877}{648} \\
& + \frac{323}{18}\zeta_2 + \frac{89}{9}\zeta_3 + 24\ln 2\zeta_2 - \frac{47}{5}\zeta_2^2\Big] + n_l C_F\Big[-\frac{2}{9}L_\mu^3 - \frac{13}{9}L_\mu^2 + \left(-\frac{77}{27} - \frac{8}{3}\zeta_2\right)L_\mu \\
& - \frac{1541}{324} - \frac{37}{9}\zeta_2 - \frac{26}{9}\zeta_3\Big],
\end{aligned}
$$
(C.7)

$$
\begin{aligned}
\mathcal{Z}_{[t]}^{(2),t} = & C_F T_F \Bigg[\frac{2}{\epsilon^3} + \frac{1}{\epsilon^2}\left(\frac{4}{3}L_\mu + \frac{8}{9}\right) + \frac{1}{\epsilon}\left(\frac{4}{9}L_\mu - \frac{65}{27} - 2\zeta_2\right) - \frac{4}{9}L_\mu^3 - \frac{2}{9}L_\mu^2 \\
& - \left(\frac{274}{27} + \frac{16\zeta_2}{3}\right)L_\mu + \frac{5107}{162} - \frac{70\zeta_2}{9} - \frac{4\zeta_3}{9}\Bigg].
\end{aligned}
$$
(C.8)

Finally, $\mathcal{Z}$-factors for gluons up to NNLO are given by

$$
\begin{aligned}
\mathcal{Z}_{[g]}^{(1)} &= \left\{ -\frac{2}{3\epsilon} - \frac{2}{3}L_\mu + \epsilon\left(-\frac{1}{3}L_\mu^2 - \frac{\zeta_2}{3}\right) + \epsilon^2\left(-\frac{1}{9}L_\mu^3 - \frac{\zeta_2}{3}L_\mu + \frac{2\zeta_3}{9}\right)\right\}, \\
\mathcal{Z}_{[g]}^{(2)} &= \left(\mathcal{Z}_{[g]}^{(1)}\right)^2 + \frac{4}{3\epsilon}(n_h + n_l)T_F \mathcal{Z}_{[g]}^{(1)} + \mathcal{Z}_{[g]}^{(2),t}.
\end{aligned}
$$

where $\mathcal{Z}_{[g]}^{(2),t}$ denotes the contribution from a loop insertion of top quark,

$$
\begin{aligned}
\mathcal{Z}_{[g]}^{(2),t} = C_A T_F \left(\frac{\mu^2}{m_t^2}\right)^{2\epsilon} &\left[\frac{2}{\epsilon^3} + \frac{34}{9\epsilon^2} - \frac{2}{\epsilon}\left(\frac{22}{9}L_\mu + \frac{64}{27} - \zeta_2\right)\right. \\
&\left. + \frac{22}{9}L_\mu^2 + \frac{358}{27} + \frac{4\zeta_2}{3} - 4\zeta_3\right] - C_F T_F \left(\frac{\mu^2}{m_t^2}\right)^{2\epsilon}\left(\frac{2}{\epsilon} + 15\right).
\end{aligned} \tag{C.9}
$$

Open Access. This article is distributed under the terms of the Creative Commons Attribution License ([CC-BY4.0](#)), which permits any use, distribution and reproduction in any medium, provided the original author(s) and source are credited.

References

[1] ATLAS collaboration, *Observation of a new particle in the search for the Standard Model Higgs boson with the ATLAS detector at the LHC*, *Phys. Lett. B* **716** (2012) 1 [`arXiv:1207.7214`] [INSPIRE].

[2] CMS collaboration, *Observation of a New Boson at a Mass of 125 GeV with the CMS Experiment at the LHC*, *Phys. Lett. B* **716** (2012) 30 [`arXiv:1207.7235`] [INSPIRE].

[3] ATLAS collaboration, *Observation of Higgs boson production in association with a top quark pair at the LHC with the ATLAS detector*, *Phys. Lett. B* **784** (2018) 173 [`arXiv:1806.00425`] [INSPIRE].

[4] CMS collaboration, *Observation of $t\bar{t}H$ production*, *Phys. Rev. Lett.* **120** (2018) 231801 [`arXiv:1804.02610`] [INSPIRE].

[5] CMS collaboration, *Measurements of $t\bar{t}H$ Production and the CP Structure of the Yukawa Interaction between the Higgs Boson and Top Quark in the Diphoton Decay Channel*, *Phys. Rev. Lett.* **125** (2020) 061801 [`arXiv:2003.10866`] [INSPIRE].

[6] ATLAS collaboration, *CP Properties of Higgs Boson Interactions with Top Quarks in the $t\bar{t}H$ and tH Processes Using $H \rightarrow \gamma\gamma$ with the ATLAS Detector*, *Phys. Rev. Lett.* **125** (2020) 061802 [`arXiv:2004.04545`] [INSPIRE].

[7] M. Cepeda et al., *Report from Working Group 2: Higgs Physics at the HL-LHC and HE-LHC*, *CERN Yellow Rep. Monogr.* **7** (2019) 221 [`arXiv:1902.00134`] [INSPIRE].

[8] J.N. Ng and P. Zakarauskas, *A QCD Parton Calculation of Conjoined Production of Higgs Bosons and Heavy Flavors in $p\bar{p}$ Collision*, *Phys. Rev. D* **29** (1984) 876 [INSPIRE].

[9] Z. Kunszt, *Associated Production of Heavy Higgs Boson with Top Quarks*, *Nucl. Phys. B* **247** (1984) 339 [INSPIRE].

[10] W. Beenakker et al., *Higgs radiation off top quarks at the Tevatron and the LHC*, *Phys. Rev. Lett.* **87** (2001) 201805 [`hep-ph/0107081`] [INSPIRE].

[11] W. Beenakker et al., *NLO QCD corrections to $t\bar{t}$ H production in hadron collisions*, *Nucl. Phys. B* **653** (2003) 151 [`hep-ph/0211352`] [INSPIRE].

[12] L. Reina and S. Dawson, *Next-to-leading order results for $t\bar{t}$ h production at the Tevatron*, *Phys. Rev. Lett.* **87** (2001) 201804 [`hep-ph/0107101`] [INSPIRE].

[13] L. Reina, S. Dawson and D. Wackeroth, *QCD corrections to associated $t\bar{t}h$ production at the Tevatron*, *Phys. Rev. D* **65** (2002) 053017 [`hep-ph/0109066`] [INSPIRE].

[14] S. Dawson, L.H. Orr, L. Reina and D. Wackeroth, *Associated top quark Higgs boson production at the LHC*, *Phys. Rev. D* **67** (2003) 071503 [hep-ph/0211438] [INSPIRE].

[15] S. Dawson et al., *Associated Higgs production with top quarks at the large hadron collider: NLO QCD corrections*, *Phys. Rev. D* **68** (2003) 034022 [hep-ph/0305087] [INSPIRE].

[16] R. Frederix et al., *Scalar and pseudoscalar Higgs production in association with a top-antitop pair*, *Phys. Lett. B* **701** (2011) 427 [arXiv:1104.5613] [INSPIRE].

[17] M.V. Garzelli, A. Kardos, C.G. Papadopoulos and Z. Trocsanyi, *Standard Model Higgs boson production in association with a top anti-top pair at NLO with parton showering*, *EPL* **96** (2011) 11001 [arXiv:1108.0387] [INSPIRE].

[18] H.B. Hartanto, B. Jager, L. Reina and D. Wackeroth, *Higgs boson production in association with top quarks in the POWHEG BOX*, *Phys. Rev. D* **91** (2015) 094003 [arXiv:1501.04498] [INSPIRE].

[19] S. Frixione et al., *Weak corrections to Higgs hadroproduction in association with a top-quark pair*, *JHEP* **09** (2014) 065 [arXiv:1407.0823] [INSPIRE].

[20] Y. Zhang et al., *QCD NLO and EW NLO corrections to t̄tH production with top quark decays at hadron collider*, *Phys. Lett. B* **738** (2014) 1 [arXiv:1407.1110] [INSPIRE].

[21] S. Frixione et al., *Electroweak and QCD corrections to top-pair hadroproduction in association with heavy bosons*, *JHEP* **06** (2015) 184 [arXiv:1504.03446] [INSPIRE].

[22] A. Denner and R. Feger, *NLO QCD corrections to off-shell top-antitop production with leptonic decays in association with a Higgs boson at the LHC*, *JHEP* **11** (2015) 209 [arXiv:1506.07448] [INSPIRE].

[23] A. Denner, J.-N. Lang and M. Pellen, *Full NLO QCD corrections to off-shell t̄tbb̄ production*, *Phys. Rev. D* **104** (2021) 056018 [arXiv:2008.00918] [INSPIRE].

[24] D. Stremmer and M. Worek, *Production and decay of the Higgs boson in association with top quarks*, *JHEP* **02** (2022) 196 [arXiv:2111.01427] [INSPIRE].

[25] G. Bevilacqua et al., *t̄tbb̄ at the LHC: On the size of off-shell effects and prompt b-jet identification*, *Phys. Rev. D* **107** (2023) 014028 [arXiv:2202.11186] [INSPIRE].

[26] A. Kulesza, L. Motyka, T. Stebel and V. Theeuwes, *Soft gluon resummation for associated t̄tH production at the LHC*, *JHEP* **03** (2016) 065 [arXiv:1509.02780] [INSPIRE].

[27] A. Broggio et al., *Associated production of a top pair and a Higgs boson beyond NLO*, *JHEP* **03** (2016) 124 [arXiv:1510.01914] [INSPIRE].

[28] A. Broggio, A. Ferroglia, B.D. Pecjak and L.L. Yang, *NNLL resummation for the associated production of a top pair and a Higgs boson at the LHC*, *JHEP* **02** (2017) 126 [arXiv:1611.00049] [INSPIRE].

[29] A. Kulesza, L. Motyka, T. Stebel and V. Theeuwes, *Associated t̄tH production at the LHC: Theoretical predictions at NLO+NNLL accuracy*, *Phys. Rev. D* **97** (2018) 114007 [arXiv:1704.03363] [INSPIRE].

[30] A. Broggio et al., *Top-quark pair hadroproduction in association with a heavy boson at NLO+NNLL including EW corrections*, *JHEP* **08** (2019) 039 [arXiv:1907.04343] [INSPIRE].

[31] W.-L. Ju and L.L. Yang, *Resummation of soft and Coulomb corrections for t̄th production at the LHC*, *JHEP* **06** (2019) 050 [arXiv:1904.08744] [INSPIRE].

[32] A. Kulesza et al., *Associated top quark pair production with a heavy boson: differential cross sections at NLO+NNLL accuracy*, *Eur. Phys. J. C* **80** (2020) 428 [arXiv:2001.03031] [INSPIRE].

[33] A. Denner, J.-N. Lang, M. Pellen and S. Uccirati, *Higgs production in association with off-shell top-antitop pairs at NLO EW and QCD at the LHC*, *JHEP* **02** (2017) 053 [arXiv:1612.07138] [INSPIRE].

[34] F. Maltoni, E. Vryonidou and C. Zhang, *Higgs production in association with a top-antitop pair in the Standard Model Effective Field Theory at NLO in QCD*, *JHEP* **10** (2016) 123 [arXiv:1607.05330] [INSPIRE].

[35] J. Chen et al., *Two-loop infrared singularities in the production of a Higgs boson associated with a top-quark pair*, *JHEP* **04** (2022) 025 [arXiv:2202.02913] [INSPIRE].

[36] F. Buccioni, P.A. Kreer, X. Liu and L. Tancredi, *One loop QCD corrections to $gg \to t\bar{t}H$ at $\mathcal{O}\left(\epsilon^2\right)$*, *JHEP* **03** (2024) 093 [arXiv:2312.10015] [INSPIRE].

[37] S. Catani, I. Fabre, M. Grazzini and S. Kallweit, *$t\bar{t}H$ production at NNLO: the flavour off-diagonal channels*, *Eur. Phys. J. C* **81** (2021) 491 [arXiv:2102.03256] [INSPIRE].

[38] B. Agarwal et al., *Two-loop amplitudes for $t\bar{t}H$ production: the quark-initiated N_f-part*, *JHEP* **05** (2024) 013 [*Erratum ibid.* **06** (2024) 142] [arXiv:2402.03301] [INSPIRE].

[39] S. Catani et al., *Higgs Boson Production in Association with a Top-Antitop Quark Pair in Next-to-Next-to-Leading Order QCD*, *Phys. Rev. Lett.* **130** (2023) 111902 [arXiv:2210.07846] [INSPIRE].

[40] F. Febres Cordero et al., *Two-Loop Master Integrals for Leading-Color $pp \to t\bar{t}H$ Amplitudes with a Light-Quark Loop*, arXiv:2312.08131 [INSPIRE].

[41] A. Mitov and S. Moch, *The singular behavior of massive QCD amplitudes*, *JHEP* **05** (2007) 001 [hep-ph/0612149] [INSPIRE].

[42] T. Becher and K. Melnikov, *Two-loop QED corrections to Bhabha scattering*, *JHEP* **06** (2007) 084 [arXiv:0704.3582] [INSPIRE].

[43] T. Engel, C. Gnendiger, A. Signer and Y. Ulrich, *Small-mass effects in heavy-to-light form factors*, *JHEP* **02** (2019) 118 [arXiv:1811.06461] [INSPIRE].

[44] G. Wang, T. Xia, L.L. Yang and X. Ye, *On the high-energy behavior of massive QCD amplitudes*, *JHEP* **05** (2024) 082 [arXiv:2312.12242] [INSPIRE].

[45] J. Böhm et al., *Complete integration-by-parts reductions of the non-planar hexagon-box via module intersections*, *JHEP* **09** (2018) 024 [arXiv:1805.01873] [INSPIRE].

[46] D. Bendle et al., *Integration-by-parts reductions of Feynman integrals using Singular and GPI-Space*, *JHEP* **02** (2020) 079 [arXiv:1908.04301] [INSPIRE].

[47] J. Boehm et al., *IBP reduction coefficients made simple*, *JHEP* **12** (2020) 054 [arXiv:2008.13194] [INSPIRE].

[48] D. Bendle et al., *pfd-parallel, a Singular/GPI-Space package for massively parallel multivariate partial fractioning*, *Comput. Phys. Commun.* **294** (2024) 108942 [arXiv:2104.06866] [INSPIRE].

[49] Z. Wu et al., *NeatIBP 1.0, a package generating small-size integration-by-parts relations for Feynman integrals*, *Comput. Phys. Commun.* **295** (2024) 108999 [arXiv:2305.08783] [INSPIRE].

[50] X. Guan, X. Liu and Y.-Q. Ma, *Complete reduction of integrals in two-loop five-light-parton scattering amplitudes*, *Chin. Phys. C* **44** (2020) 093106 [arXiv:1912.09294] [INSPIRE].

[51] M. Heller and A. von Manteuffel, *MultivariateApart: Generalized partial fractions*, *Comput. Phys. Commun.* **271** (2022) 108174 [`arXiv:2101.08283`] [ɪɴSPIRE].

[52] T. Gehrmann, J.M. Henn and N.A. Lo Presti, *Analytic form of the two-loop planar five-gluon all-plus-helicity amplitude in QCD*, *Phys. Rev. Lett.* **116** (2016) 062001 [*Erratum ibid.* **116** (2016) 189903] [`arXiv:1511.05409`] [ɪɴSPIRE].

[53] C.G. Papadopoulos, D. Tommasini and C. Wever, *The Pentabox Master Integrals with the Simplified Differential Equations approach*, *JHEP* **04** (2016) 078 [`arXiv:1511.09404`] [ɪɴSPIRE].

[54] T. Gehrmann, J.M. Henn and N.A. Lo Presti, *Pentagon functions for massless planar scattering amplitudes*, *JHEP* **10** (2018) 103 [`arXiv:1807.09812`] [ɪɴSPIRE].

[55] D. Chicherin et al., *Analytic result for the nonplanar hexa-box integrals*, *JHEP* **03** (2019) 042 [`arXiv:1809.06240`] [ɪɴSPIRE].

[56] S. Abreu, B. Page and M. Zeng, *Differential equations from unitarity cuts: nonplanar hexa-box integrals*, *JHEP* **01** (2019) 006 [`arXiv:1807.11522`] [ɪɴSPIRE].

[57] S. Abreu et al., *The two-loop five-point amplitude in $\mathcal{N} = 4$ super-Yang-Mills theory*, *Phys. Rev. Lett.* **122** (2019) 121603 [`arXiv:1812.08941`] [ɪɴSPIRE].

[58] D. Chicherin et al., *All Master Integrals for Three-Jet Production at Next-to-Next-to-Leading Order*, *Phys. Rev. Lett.* **123** (2019) 041603 [`arXiv:1812.11160`] [ɪɴSPIRE].

[59] S. Badger et al., *Analytic form of the full two-loop five-gluon all-plus helicity amplitude*, *Phys. Rev. Lett.* **123** (2019) 071601 [`arXiv:1905.03733`] [ɪɴSPIRE].

[60] S. Catani and M.H. Seymour, *The dipole formalism for the calculation of QCD jet cross-sections at next-to-leading order*, *Phys. Lett. B* **378** (1996) 287 [`hep-ph/9602277`] [ɪɴSPIRE].

[61] S. Catani and M.H. Seymour, *A general algorithm for calculating jet cross-sections in NLO QCD*, *Nucl. Phys. B* **485** (1997) 291 [`hep-ph/9605323`] [ɪɴSPIRE].

[62] M. Czakon, A. Mitov and S. Moch, *Heavy-quark production in massless quark scattering at two loops in QCD*, *Phys. Lett. B* **651** (2007) 147 [`arXiv:0705.1975`] [ɪɴSPIRE].

[63] M. Czakon, A. Mitov and S. Moch, *Heavy-quark production in gluon fusion at two loops in QCD*, *Nucl. Phys. B* **798** (2008) 210 [`arXiv:0707.4139`] [ɪɴSPIRE].

[64] H. Gervais, *Soft Photon Theorem for High Energy Amplitudes in Yukawa and Scalar Theories*, *Phys. Rev. D* **95** (2017) 125009 [`arXiv:1704.00806`] [ɪɴSPIRE].

[65] E. Laenen et al., *Towards all-order factorization of QED amplitudes at next-to-leading power*, *Phys. Rev. D* **103** (2021) 034022 [`arXiv:2008.01736`] [ɪɴSPIRE].

[66] V.S. Fadin and R.N. Lee, *Two-loop radiative corrections to $e^+e^- \to \gamma\gamma^*$ cross section*, *JHEP* **11** (2023) 148 [`arXiv:2308.09479`] [ɪɴSPIRE].

[67] T. Hahn, *Generating Feynman diagrams and amplitudes with FeynArts 3*, *Comput. Phys. Commun.* **140** (2001) 418 [`hep-ph/0012260`] [ɪɴSPIRE].

[68] R. Mertig, M. Bohm and A. Denner, *FEYN CALC: Computer algebraic calculation of Feynman amplitudes*, *Comput. Phys. Commun.* **64** (1991) 345 [ɪɴSPIRE].

[69] V. Shtabovenko, R. Mertig and F. Orellana, *New Developments in FeynCalc 9.0*, *Comput. Phys. Commun.* **207** (2016) 432 [`arXiv:1601.01167`] [ɪɴSPIRE].

[70] V. Shtabovenko, R. Mertig and F. Orellana, *FeynCalc 9.3: New features and improvements*, *Comput. Phys. Commun.* **256** (2020) 107478 [`arXiv:2001.04407`] [ɪɴSPIRE].

[71] J.A.M. Vermaseren, *New features of FORM*, `math-ph/0010025` [ɪɴSPIRE].

[72] D. Chicherin and V. Sotnikov, *Pentagon Functions for Scattering of Five Massless Particles*, *JHEP* **12** (2020) 167 [arXiv:2009.07803] [InSPIRE].

[73] P. Maierhöfer, J. Usovitsch and P. Uwer, *Kira — A Feynman integral reduction program*, *Comput. Phys. Commun.* **230** (2018) 99 [arXiv:1705.05610] [InSPIRE].

[74] J. Klappert, F. Lange, P. Maierhöfer and J. Usovitsch, *Integral reduction with Kira 2.0 and finite field methods*, *Comput. Phys. Commun.* **266** (2021) 108024 [arXiv:2008.06494] [InSPIRE].

[75] J. Klappert and F. Lange, *Reconstructing rational functions with FireFly*, *Comput. Phys. Commun.* **247** (2020) 106951 [arXiv:1904.00009] [InSPIRE].

[76] J. Klappert, S.Y. Klein and F. Lange, *Interpolation of dense and sparse rational functions and other improvements in FireFly*, *Comput. Phys. Commun.* **264** (2021) 107968 [arXiv:2004.01463] [InSPIRE].

[77] B. Mele and P. Nason, *The fragmentation function for heavy quarks in QCD*, *Nucl. Phys. B* **361** (1991) 626 [InSPIRE].

[78] A. Ferroglia, B.D. Pecjak and L.L. Yang, *Soft-gluon resummation for boosted top-quark production at hadron colliders*, *Phys. Rev. D* **86** (2012) 034010 [arXiv:1205.3662] [InSPIRE].

[79] A. Ferroglia, S. Marzani, B.D. Pecjak and L.L. Yang, *Boosted top production: factorization and resummation for single-particle inclusive distributions*, *JHEP* **01** (2014) 028 [arXiv:1310.3836] [InSPIRE].

[80] B.D. Pecjak, D.J. Scott, X. Wang and L.L. Yang, *Resummed differential cross sections for top-quark pairs at the LHC*, *Phys. Rev. Lett.* **116** (2016) 202001 [arXiv:1601.07020] [InSPIRE].

[81] M. Czakon et al., *Resummation for (boosted) top-quark pair production at NNLO+NNLL' in QCD*, *JHEP* **05** (2018) 149 [arXiv:1803.07623] [InSPIRE].

[82] J. Alwall et al., *The automated computation of tree-level and next-to-leading order differential cross sections, and their matching to parton shower simulations*, *JHEP* **07** (2014) 079 [arXiv:1405.0301] [InSPIRE].

[83] R. Frederix et al., *The automation of next-to-leading order electroweak calculations*, *JHEP* **11** (2018) 085 [*Erratum ibid.* **11** (2021) 085] [arXiv:1804.10017] [InSPIRE].

[84] GoSam collaboration, *Automated One-Loop Calculations with GoSam*, *Eur. Phys. J. C* **72** (2012) 1889 [arXiv:1111.2034] [InSPIRE].

[85] GoSam collaboration, *GOSAM-2.0: a tool for automated one-loop calculations within the Standard Model and beyond*, *Eur. Phys. J. C* **74** (2014) 3001 [arXiv:1404.7096] [InSPIRE].

[86] F. Buccioni et al., *OpenLoops 2*, *Eur. Phys. J. C* **79** (2019) 866 [arXiv:1907.13071] [InSPIRE].

[87] F. Cascioli, P. Maierhöfer and S. Pozzorini, *Scattering Amplitudes with Open Loops*, *Phys. Rev. Lett.* **108** (2012) 111601 [arXiv:1111.5206] [InSPIRE].

[88] F. Buccioni, S. Pozzorini and M. Zoller, *On-the-fly reduction of open loops*, *Eur. Phys. J. C* **78** (2018) 70 [arXiv:1710.11452] [InSPIRE].

[89] S. Actis et al., *RECOLA: REcursive Computation of One-Loop Amplitudes*, *Comput. Phys. Commun.* **214** (2017) 140 [arXiv:1605.01090] [InSPIRE].

[90] A. Denner, J.-N. Lang and S. Uccirati, *Recola2: REcursive Computation of One-Loop Amplitudes 2*, *Comput. Phys. Commun.* **224** (2018) 346 [arXiv:1711.07388] [InSPIRE].

[91] A. Ferroglia, M. Neubert, B.D. Pecjak and L.L. Yang, *Two-loop divergences of massive scattering amplitudes in non-abelian gauge theories*, *JHEP* **11** (2009) 062 [arXiv:0908.3676] [InSPIRE].